THESIS

WETLAND EXTENT FROM A TOPOGRAPHIC INDEX, WETLAND'S IMPACT ON LAND SURFACE FLUXES AND A MODEL OF CH_4 EXCHANGE

Submitted by

Parker Mayo Kraus

Department of Atmospheric Science

In partial fulfillment of the requirements

For the Degree of Master of Science

Colorado State University

Fort Collins, Colorado

Fall 2011

Master's Committee:

Advisor: A. Scott Denning
Joe von Fischer
Colette L. Heald
Department Head: Jeffrey L. Collett, Jr.

ABSTRACT

WETLAND EXTENT FROM A TOPOGRAPHIC INDEX, WETLAND'S IMPACT ON LAND SURFACE FLUXES AND A MODEL OF CH_4 EXCHANGE

A method of estimating wetland extent is developed for use in the land surface components of climate/atmospheric models. The approach is developed within the Simple Biosphere Model, SiB, but is intended as a flexible framework applicable to other models. It uses the topographic index, $\ln(a/\tan\beta)$, to calculate wetland area as a function of regional hydrologic characteristics and model water content.

The calculation of the index is discussed, alternatives to the formally required depression-less DEM are investigated and an approach utilizing a smoothed DEM is adopted. Modeled water content is used to establish a point of saturation on the histogram of topographic index, which varies as modeled water content varies, providing estimates of the wetland fraction over time. This relationship is parameterized for the WLEF-TV tower in northern Wisconsin, and tested at locations in Florida and Louisiana. The method of parameterization is found to be acceptable, but site specific parameterization is desirable.

Applications of the model are developed. Sensible and latent heat fluxes and net ecosystem exchange modeled with SiB2.5 at the WLEF site are reevaluated with SiB3 and compared to observations. The wetland area model is used to scale SiB3 estimates of these fluxes using a saturated, "wetland," version of the model. Scaling improves estimates, but is overshadowed by errors introduced to the model by changes in the method by which water stress is calculated in SiB.

A simple model of methanogenesis and methanotrophy employing predictions of wetland area is proposed and incorporated in SiB. The dynamics of this model are explored in relation to the temperature dependence, Q_{10}, of methanogenic respiration and conditions of equilibrium. Inspection of the model suggests a seasonal cycle of methane flux with summertime emission and fall and springtime consumption. Estimates from the model are compared with Modified Bowen Ratio, MBR, estimates of methane flux based on observations at WLEF site. Observed fluxes offer some empirical constraint on methanogenic Q_{10}, but uncertainties in the methane flux preclude assessment of the variability of wetland area. Methane consumption is overrepresented in the predicted seasonal cycle of methane flux due to the simplified representation of methanotrophy in the model, but the essential expected behavior is confirmed.

Verification of model parameters beyond the WLEF is necessary, though the feasibility of modeling variable wetland extent using the topographic index is demonstrated. Applications of the calculation for representing sub-grid scale soil moisture variability and saturated zone biogeochemistry appear promising for use in atmosphere-coupled regional or global model runs.

ACKNOWLEDGEMENTS

I thank my advisor Professor Scott Denning for supporting this work and the Center for Multiscale Modeling of Atmospheric Processes for funding it. Thanks also to Isaac Medina for his help and Ian Baker for his guidance. I was led to this university, department and degree by my undergraduate advisor at Colorado College, Professor Howard Drossman, whom I thank. And thank you, thorough reader.

TABLE OF CONTENTS

1. THE TOPOGRAPHIC INDEX

Origin and derivation of the topographic index

The TOPMODEL Topographic Index of Hydrologic Similarity, or simply the topographic index, *TI*, and various other associated indices have been derived and utilized since the development of the TOPMODEL hydrologic framework [*Beven and Kirkby*, 1979]. The topographic index describes geographic points which behave in hydrologically identical fashions; given the assumptions made in the derivation of the index [*Beven et al.*, 1995].This behavioral consistency allows a heterogeneous landscape to be treated with histogram of the index, or a function thereof, once it has been computed from topographic data.

Considerable effort has gone into investigation of the topographic index's calculation and its parameter space [*Quinn et al.*, 1995; *Sivapalan et al.*, 1987]. Some have considered and relaxed the assumptions made in the framework [*Ambroise et al.*, 1996; *Duan and Miller*, 1997]. Others have investigated the scale dependence of the model and the importance of fidelity to hydrologic basin shape [*Ducharne*, 2009; *Wolock and Price*, 1994].

What follows is a description of the calculation of saturated area in the TOPMODEL framework, including the derivation of the topographic index. This discussion closely follows the derivation in [*Ducharne*, 2009]. A more complete derivation of the TOPMODEL framework, rather then just the calculation of saturated area, may be found in [*Franchini et al.*, 1996]. And the concurrent derivations of several indices for different assumed transmissivity profiles in [*Ambroise et al.*, 1996], may be further instructive.

There is little symbolic consistency between papers using the topographic index. Publications may refer to it: χ, κ, Γ, γ, *TI* and ζ among others. Some papers have adopted different symbols for the basin average topographic index and the local topographic index. The confusion is not helped by the fact that the framework may be constructed with respect either to water table depth or to the storage deficit. Nor is it clarified by the ambiguity of terms like "conductivity", "permeability" and "transmissivity" to non-specialists. Here, water table depth is used and the choices of symbols mostly follow the choices of [*Beven et al.*, 1995].

Four basic assumptions are made within the TOPMODEL framework.

H1: Recharge to the water table, R, is uniform throughout the catchment.

H2: Water table dynamics are approximated by successive steady states.

H3: The local hydraulic gradient, i_i, is approximated by the local surface slope, $\tan(\beta)$.

H4: The saturated hydraulic conductivity, K_s, is a uniform function of depth throughout the catchment.

H1 requires that infiltrating water reach the water table at the same time, no matter how far below or even above the surface the local water table is at that time. It also means that heterogeneous rainfall or runoff from adjoining catchments cannot be considered.

H2 states that within the water table, local discharge, Q_i, in m^3/s, is equal to the recharge, R, in m/s, from the upstream area, A_i, in m^2 , at every timestep:

$$Q_i = A_i R . \tag{1}$$

Compare with Darcy's Law:

$$Q_i = L_i T_i i_i , \tag{2}$$

stating that the local discharge is equal to the gridcell length, L_i, in m, multiplied by the local transmissivity, T_i, in m^2/s, multiplied by the hydraulic gradient, i_i, which is unitless.

By H3, the local hydraulic gradient is assumed equal to the local topographic slope, so

$$Q_i = L_i T_i \tan(\beta_i) . \tag{3}$$

Transmissivity is defined as the integral of the saturated hydraulic conductivity, K_s, in m/s, through the saturated portion of the column, beginning at z_i, the (positive) depth to the water table,

$$T_i \equiv \int_{z_i}^{\infty} K_s(z)\, dz . \tag{4}$$

By H4, the saturated hydraulic conductivity, K_s, must be a constant function over the domain. The usual choice is an exponential function decreasing with depth:

$$K_s(z) = K_0 e^{(-fz)}, \tag{5}$$

where f is a parameter in m^{-1}, and the fully saturated hydraulic conductivity $K_0 = K_s(0)$. Equation (4) and equation (5) may be combined, and the integral solved:

$$T_i = K_0 \int_{z_i}^{\infty} e^{(-fz)}\, dz = \frac{K_0}{f} e^{(-fz)}. \tag{6}$$

Consider the first form of equation (6), when the column is fully saturated z_i is equal to zero. In that case, the integrated term reduces to $1/f$, so the saturated soil transmissivity, T_0, is equal to K_0/f. Therefore, T_0 may be substituted into the second form of equation (6), and combination with equation (3) gives a statement for the discharge equivalent to equation (1):

$$Q_i = L_i T_0 e^{-fz_i} \tan(\beta_i) = A_i R. \tag{7}$$

The depth to the local water table, z_i, is unknown, it may be solved for by rearranging:

$$z_i = -\frac{1}{f} \ln\left(\frac{a_i R}{T_0 \tan(\beta_i)} \right), \tag{8}$$

where $a_i = A_i / L_i$, the upstream area per unit length in m. The logarithm may be split:

$$z_i = -\frac{1}{f}\left(\ln\frac{R}{T_0} + \ln\frac{a_i}{\tan(\beta_i)} \right). \tag{9}$$

The second term inside the parenthesis is the only one which varies within the catchment. Therefore, it describes the hydrological characteristics of each point within the catchment. It is the topographic index, TI:

$$TI_i = \ln \frac{a_i}{\tan(\beta_i)}, \tag{10}$$

in units of ln(m). The catchment mean water table depth is defined as,

$$\bar{z} = \frac{1}{A}\int_A z_i dA\,. \tag{11}$$

Substituting with z_i from equation (9) gives:

$$\bar{z} = -\frac{1}{fA}\int_A \ln\left(\frac{R}{T_0}\right) + \ln\left(\frac{a_i}{\tan(\beta_i)}\right) dA\,. \tag{12}$$

Note that R and T_0 are constant, so the integral in equation (12) may be reduced to the catchment average topographic index, $\overline{TI}$. By substitution for R from equation (7), equation (12) may be rewritten as:

$$\bar{z} = \frac{1}{f}\left[-\ln\left(\frac{e^{-f z_i}\tan(\beta_i)}{a_i}\right) - \overline{TI}\right], \tag{13}$$

which reduces to:

$$\bar{z} - z_i = -\frac{1}{f}\left(TI_i - \overline{TI}\right). \tag{14}$$

Points are saturated if z_i is less than or equal to zero, or equivalently by rearrangement of equation (14) if:

$$TI_i \geq \overline{TI} + f\bar{z}\,, \tag{15}$$

for any given mean water table depth.

Calculation of the topographic index

The topographic index defines the hydrologic characteristics of a point as the relationship between two spatial parameters; upstream area and slope. Level, low-lying terrain is more likely to be inundated and has a high topographic index, conversely, steep, elevated terrain is less likely to be inundated and has a low topographic index.

While the *TI* is conceptually straightforward, several complications arise in its computation. The first concern is what is meant by the slope, a definition that also affects the estimate of the upstream area. In this study the multiple flow direction algorithm of [*Quinn et al.*, 1991] and updated by [*Stockli et al.*, 2007] is used, in which the local slope is determined by the weighted average of the downhill slopes of the eight possible flow directions on a square grid. Other definitions are possible, some incorporate the uphill slopes as well as the downhill slopes [*Western et al.*, 1999], others may use singly directional flow [*Wolock and Price*, 1994], still others compute the slope to the nearest watercourse known from maps or otherwise computed [*Merot et al.*, 2003]. A comparison of several methods of calculating slopes and upstream areas is given in [*Erskine et al.*, 2006], and shown to impact both maps and frequency distributions of the topographic index.

Another concern is the scale dependence of the topographic index. The TOPMODEL framework was developed for small catchments, ~8-10 km^2, with very small, 5-10 meter, grid-spacing. Maps and frequency distributions of the topographic

index are seen to vary between Digital Elevation Models, DEMs, with 5, 10, 25 and 50 meter grid-spacing [*Quinn et al.*, 1995]. The utility of the topographic index using maps with larger grid-spacing, 30 and 90 meter, has been demonstrated by [*Wolock and Price*, 1994] and 100 and 1,000 meter by [*Wolock and McCabe*, 2000]. The unusual unit of the topographic index, ln(m), introduces an additional resolution dependence to the index, resulting in mean *TI* values increasing logarithmically as resolution is reduced. A dimensionless index and framework is suggested by [*Ducharne*, 2009] and shown to exhibit less scale dependence than the classical index. The classical index is considered in this work, calculated using DEMs from the 30 meter USGS National Elevation Datatset [*Gesch*, 2007; *Gesch et al.*, 2002].

One further issue pertaining to the calculation of the *TI* is its dependence on the basin shape and its size. Implicit in the concept of upstream area is that a single drainage basin is modeled. If an arbitrary region is taken, upstream points may not be included and slopes at the edges are likely to be miscalculated. [*Wolock and Price*, 1994] demonstrate the viability of using DEM quadrangles to calculate the topographic index despite these limitations. Keeping with the conception that a single basin is modeled imposes both the additional difficulty of defining the basin [*Verdin and Verdin*, 1999], and the errors related to the smoothing or breaching necessary to the creation of a depression-less DEM, which must perforce represent such a basin [*Jenson and Domingue*, 1988]. The requirement of a depression-less DEM runs counter to the goal of delineating wetlands or estimating their extent, as local depressions commonly are or correspond with wetlands [*Leibowitz and Nadeau*, 2003]. Methods which minimize the alteration of DEMs for this purpose are

discussed by [*Lindsay and Creed*, 2005], an approach to compensate for gap-filling by depressing areas with known hydrologic features is discussed by [*Murphy et al.*, 2007] and a scheme for permitting local depressions in calculations of upstream area is presented by [*Arnold*, 2011].

Three methods to create better basin continuity without generating a depression-less DEM are proposed and evaluated. First, a smoothing algorithm, smooth3, from the MATLAB package is applied to the DEM for ten iterations. Second, a new DEM is created by subsampling every third point from the original DEM. Third, a new DEM is created by taking the average of every nine points in a square from the original DEM.

Subsampling may miss isolated regions of high or low relief, but those that are included will still cause problems in the calculation of the topographic index. Averaging should produce more continuous data, but still suffers from loss of resolution. Smoothing avoids the loss of resolution necessary to the other methods, but may produce level terrain which causes a numerical error in the upstream algorithm.

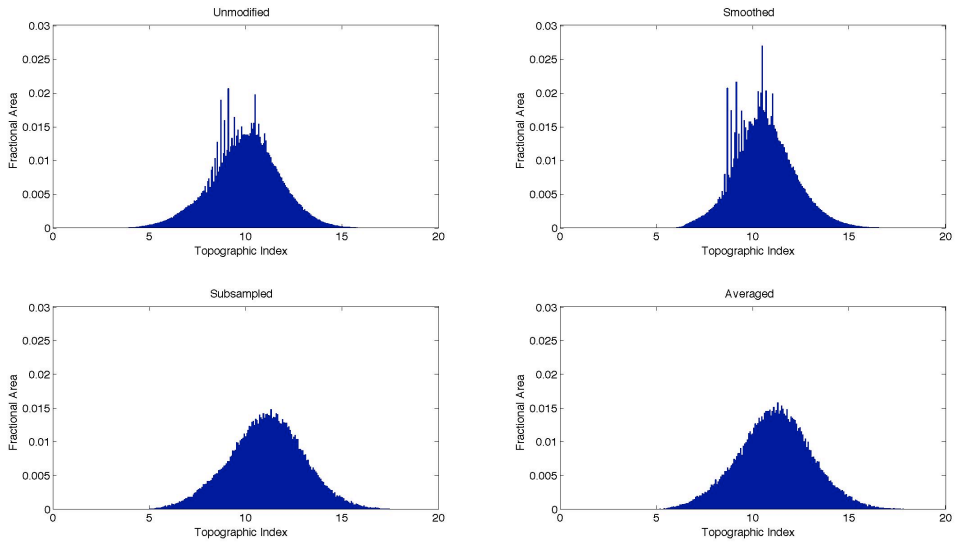

Figure 1: Histograms of the topographic index, frequency normalized to area, for a 23 x 35 km portion of the Canadian River Canyon in the Texas Panhandle with 300 bins.

Table 1: Descriptive statistics of the topographic index, Texas

	Unmodified	Smoothed	Subsampled	Averaged
Mean	9.9316	10.5323	11.0591	11.1347
Std.	1.7492	1.5457	1.9312	1.9054
Skew	-0.0803	0.3517	-0.0468	0.0202
Kurtosis	3.262	3.4038	3.0101	3.0665

The modified DEMs produces a *TI* distributions shifted toward higher values, this shift is greater with subsampled and averaged DEMs. Smoothing results in a somewhat narrower and more pointed distribution than the original, while the distributions produced after subsampling and averaging are somewhat wider and broader. The skew of the distribution is reversed by smoothing and averaging and reduced by subsampling The effects of these shifts are evident in maps of the topographic index.

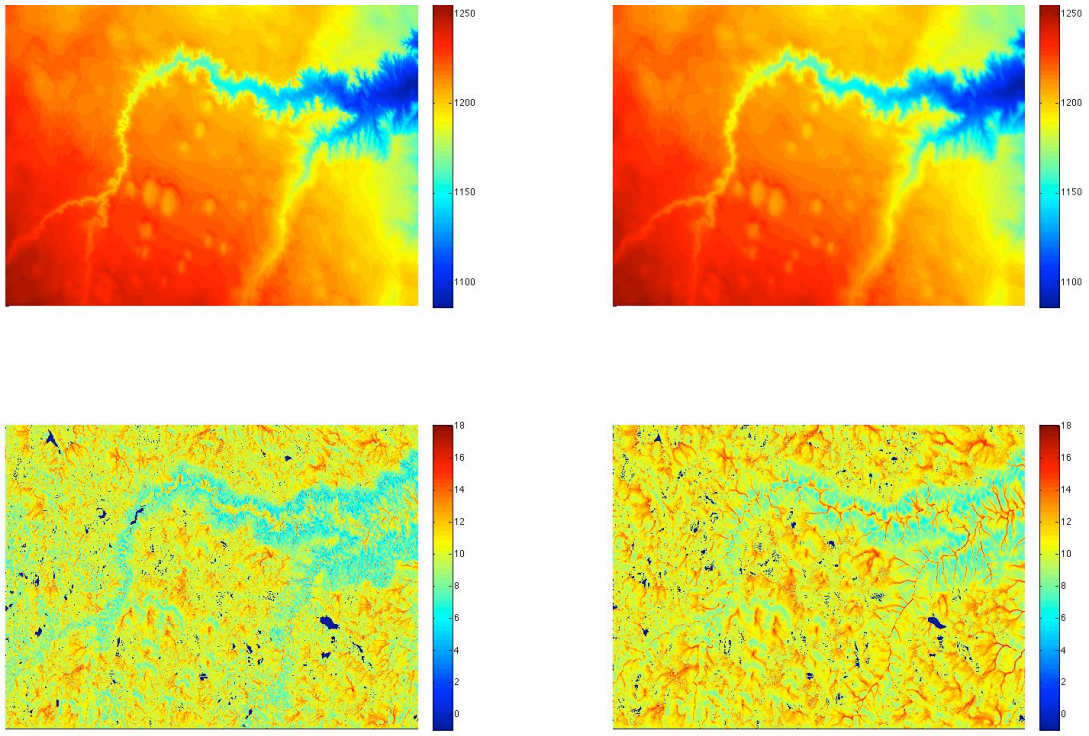

Figure 2: Top, DEM of the Canadian River Canyon, elevation in meters. Bottom, the topographic index. Left, unmodified DEM and *TI*. Right, smoothed DEM and *TI*.

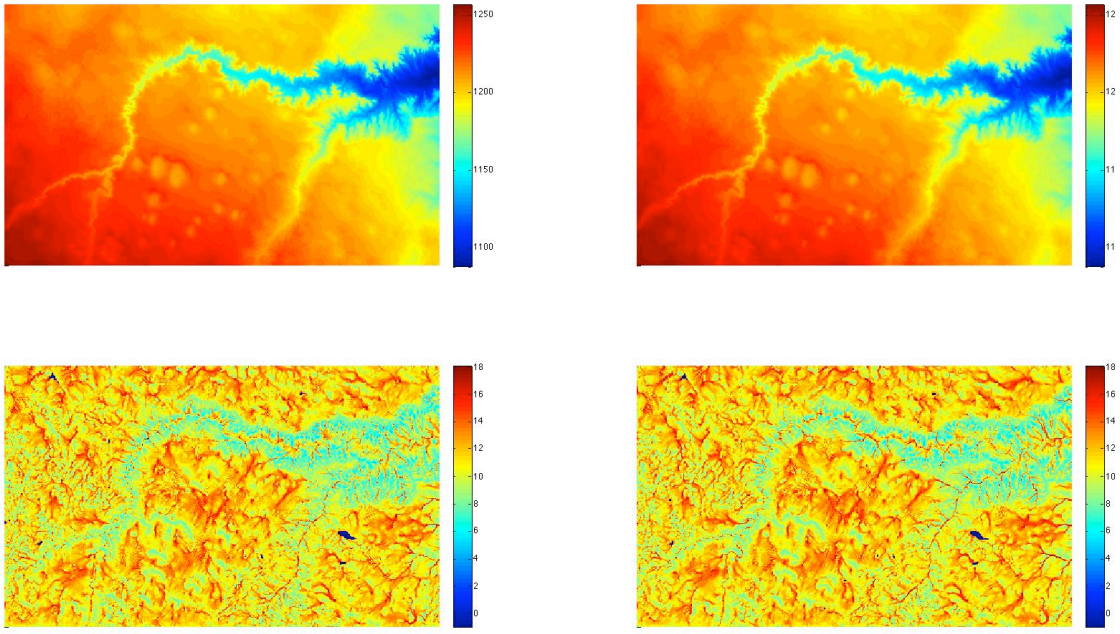

Figure 3: Top, DEM of the Canadian River Canyon, elevation in meters. Bottom, the topographic index. Left, subsampled DEM and *TI*. Right, averaged DEM and *TI*.

The *TI*s calculated from all three modified DEMs show increased connectivity between stream channels compared to the unmodified DEM. The loss of resolution in the subsampled and averaged DEMs may result in excessive estimates of the *TI* in the highlands. *TI* values of -1, dark blue, are numerical errors corresponding to perfectly level terrain, for instance over open water; these are reduced in the subsampled and averaged methods, but this may or may not be in error. Smoothing is effective in increasing basin continuity, stream channels are highlighted, as they would be with use of a depression-less DEM, but local depressions are preserved. The smoothing method exhibits little distortion of the *TI* distribution and avoids the loss of resolution in the subsampling and averaging methods. Smoothing seems effective at increasing basin continuity in a region with coherent topography and clear drainage.

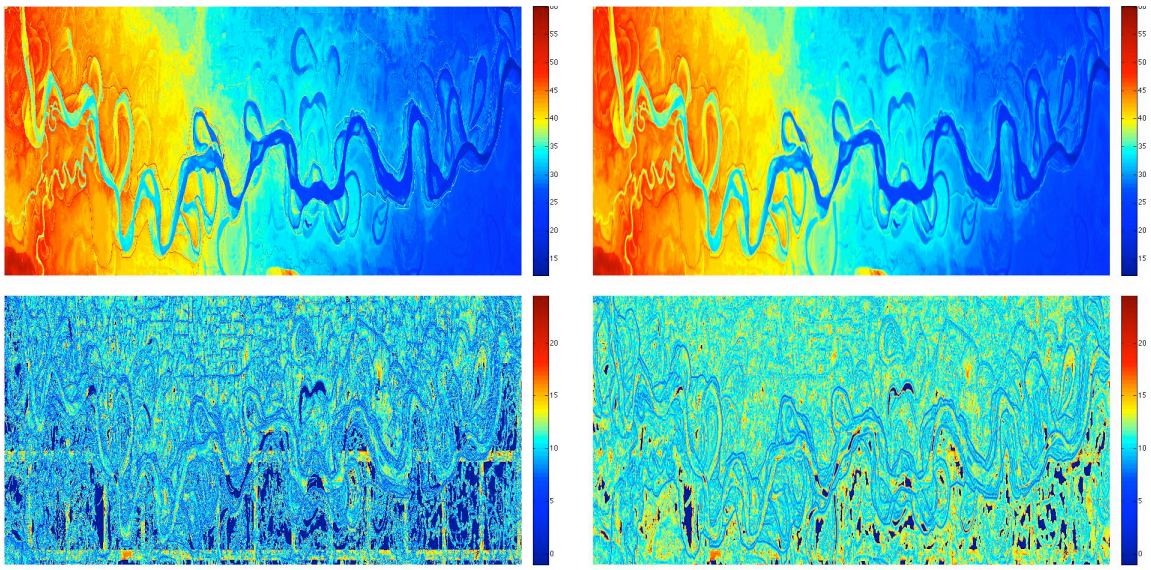

Figure 4: Top, elevations in meters, 36 x 185 km along the Mississippi river. Bottom, the topographic index. Left, unmodified DEM. Right, smoothed DEM. Linear features in the topographic index are computational errors, as are dark blue values where open water is not present.

The lower Mississippi, which possesses a low range of topographic relief and large expanses of open water, is problematic to the *TI* algorithm without modification of the DEM. The wide expanse of the Mississippi River is rarely identified as flat, while considerable areas of lowland are found to be gradient-less. Also, computational errors with distinctive linear patters arise from ambiguity in the downstream direction. Smoothing offers some improvement, less lowland is found to be gradient-less and many of the linear computational errors are eliminated. The river's levies show up as coherent features after smoothing and index values over the majority of the floodplain are reasonably increased.

With the competence of the smoothing method demonstrated, it is applied to the 9 km^2 region surrounding the WLEF-TV tower in north-central Wisconsin (45˚55'N, 90˚10'W) corresponding to be the estimated footprint of sampling instruments located on the tower at a height of 30 meters [*Werner et al.*, 2003]. The 447 meter tall tower is located within the Chequamegon National Forest, a woodland predominantly composed of Northern Hardwoods and Aspen with substantial areas of bog and forested wetland [*MacKay et al.*, 2002].

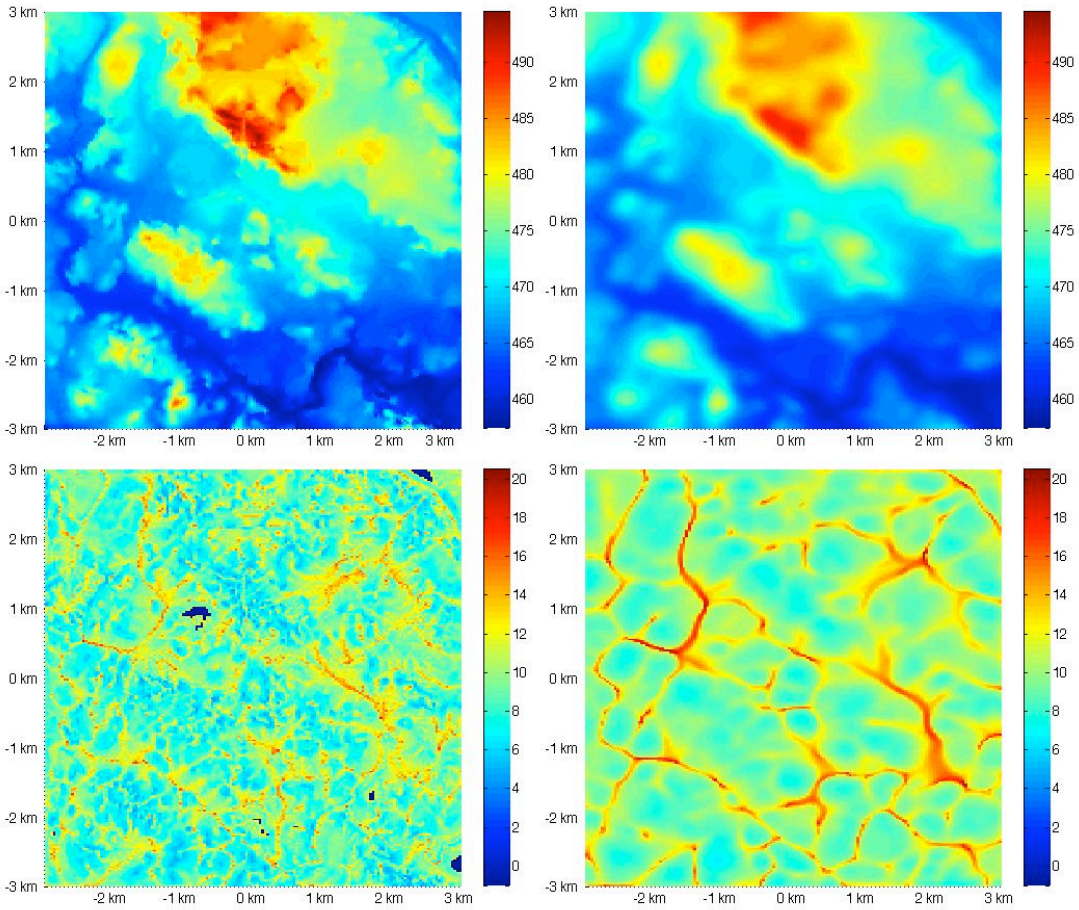

Figure 5: Top, DEM of the 9 km^2 surrounding the WLEF site, elevation in meters. Bottom, the topographic index. Left, unmodified DEM. Right, smoothed DEM. North is toward the top of the page.

The relationship between elevation and the topographic index may be considered at a much finer scale when calculated over this region as it is much smaller than those previously considered. A stream channel is seen in the DEM running down the western portion of the map, turning and then running along its southern edge. This feature is identifiable in the smoothed map of *TI*, but much harder to find in the unmodified map. It may be surprising that minor features on the DEM appear so prominently in the *TI*, but

bear in mind that steep slopes are emphasized in elevation maps and de-emphasized in maps of the *TI*.

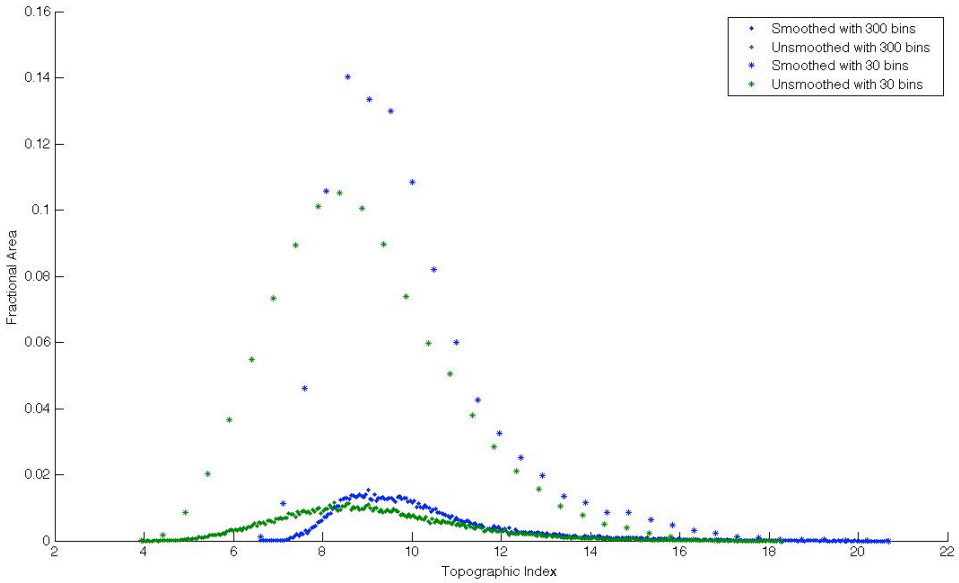

Figure 6: Histograms of the topographic index calculated for the 9 km^2 region surrounding the WLEF site. Calculated from smoothed DEM in blue, unmodified in green. Stars group topographic index values into 30 bins, diamonds into 300 bins.

The shape as well as the magnitude of distributions of *TI* depends on the binning interval. Smoothing is found to increase basin connectivity and reduce computational errors, and results in higher mean values of the topographic index and some changes in the shape of the distribution. These effects are considered advantageous, and the smoothing method is preferred to the use of unmodified DEMs..

2. WETLAND AREA

Estimating wetland extent

Wetlands comprise from 3-8% of the Earth's land surface [*Mitsch and Gosselink*, 2007]. They contain a vast share of the terrestrial carbon store, common estimates are between 20% and 30% [*Bridgham et al.*, 2006; *Mitsch and Gosselink*, 2007], though some are much higher, 50% [*Reddy and DeLaune*, 2008], 68% [*Whiting and Chanton*, 1993]. Wetlands are of additional importance as the largest natural source of atmospheric methane, contributing from 20% to 40% of global emissions [*Anderson et al.*, 2010; *IPCC*, 2007; *Wuebbles and Hayhoe*, 2002]. Much of the uncertainty in these values stem from the range of estimates of global wetland area.

The most influential estimates of global wetland extent have been derived from the compilation of observational surveys [*Aselmann and Crutzen*, 1989; *Matthews and Fung*, 1987], an effort which continues with finer resolution, more detailed classification and the incorporation of additional data [*Lehner and Döll*, 2004]. Recently developed satellite remote sensing techniques, primarily passive and active microwave backscatter [*Owe et al.*, 2008; *Prigent et al.*, 2001a], provided an additional tool for the identification of saturated ground which may help amend the chronic underestimates of wetland area

common to other remote sensing techniques [*Frey and Smith*, 2007]. One considerable advantage of observations from satellites is that nearly continuous observation permits investigation of the seasonal dynamics of wetland extent, rather than the production of static maps [*Prigent et al.*, 2001b], [*Prigent et al.*, 2007], [*Papa et al.*, 2010]. These studies indicate that most areas where soils saturate are inundated for less than half of most years and that inter-annual variability in maximum fractional inundation is greater than 20% in the majority of regions where saturation occurs and commonly greater than 40%. Temporal patterns of inundation are of critical importance to wetland biogeochemistry, and satellite estimates of saturated area have shown promise in investigating the dynamics of wetland methane generation [*Bloom et al.*, 2010], [*Ringeval et al.*, 2010], they may also prove useful for the calibration of models of wetland extent.

The TOPMODEL framework has been used in LSMs to model variable saturated areas for the purpose of improving model estimates of runoff and the representation of heterogeneous soil moisture at sub-grid scale. [*Ducharne et al.*, 1999] introduce a model with the catchment as the fundamental spatial unit to accommodate depression-less DEMs and the formalisms of TOPMODEL, further description and evaluation of this model is given in [*Koster et al.*, 2000] and [*Ducharne et al.*, 2000]. Their approach allows explicit representation of variable soil moisture, but is a considerable departure from most LSMs, for example, the model dispenses with discrete soil layers. Implementation of this model is complicated by the use of a catchment-shaped land surface domain and limited by the use of a depression-less DEM.

An alternative implementation of TOPMODEL concepts allows the representation of topographically mediated variation in soil moisture within more conventional LSMs. [*Walko et al.*, 2000] suggest that the land surface gridcell be divided into "patches" corresponding to fixed intervals of the topographic index. Water in the saturated zone flows from low *TI* patches to the higher *TI* patches at a rate proportional to the hydraulic conductivity, see equation (5). This approach is conceptually appealing, but has the drawback that water table depth is determined by the presence of saturated model soil layers, an impractical method in many models.

Rather than explicitly modeling the depth of the water table, several studies develop functions of model water content to give an approximate water table depth for use with equation (15) to estimate saturated area. [*Stieglitz et al.*, 1997] introduce a parameterized function of model soil layer, [*Chen and Kumar*, 2001] present a continuous function, [*Gedney and Cox*, 2003] and [*Niu et al.*, 2005] make additional simplifications and apply the method at global scales. Each of these studies found that catchment runoff rates could be well predicted only after empirical scaling of the hydraulic conductivity, in [*Niu et al.*, 2005] by a factor of 508. This does not indicate that the, usually observationally derived, conductivities used in LSMs are wrong so much as the role of the conductivity as a scaled parameter in the TOPMODEL framework.

Apart from the use of TOPMODEL in LSMs, the topographic index has been utilized by geographers and wetland scientists for the purpose of identifying and delineating wetlands, recently by [*Murphy et al.*, 2009] and [*Curie et al.*, 2007]. The method bares considerable resemblance to efforts to delineate wetlands using the

topographic index, only with a a constant threshold index of saturation rather than time varying, model derived value. It is appealing since topographic information is ubiquitous in comparison to pedologic maps and since remotely sensed classification consistently underestimates wetland area using normalized difference vegetation methods, [*Frey and Smith*, 2007], and photo-interpretation approaches [*MacKay et al.*, 2002; *Tiner*, 1999], particularly in forested wetlands.

[*Merot et al.*, 1995] proposed the use of a threshold index of saturation to identify wetlands as sites with waterlogged soils. They tested the predictive power of the index against pedologic maps in two catchments in Brittany, finding good qualitative agreement. Another attempt to delineate wetlands using a threshold topographic index, as well as three other indices, was performed by [*Rodhe and Seibert*, 1999] in four catchments in Sweden. They found the predictive power of the index was found to be weaker in mountainous catchments than in lowlands due to the position of the highest *TI* values in stream channels. Following the analysis in the first chapter, this likely results from their use of a depression-less DEM.

As part of a validation of the TOPMODEL framework as a hydrologic model, [*Güntner et al.*, 1999] compared model estimates of saturated area to detailed surveys of saturated area at a mountainous site in southern Germany in different seasons and weather conditions; they too found good qualitative agreement in the location of saturated areas, but overly variable model saturated areas suggested that the use of spatially varying transmissivities was necessary for accurate estimates of saturated area and runoff.

Spatial variation in soil transmissivity can be represented in TOPMODEL, in which case, T_0 becomes a part of the topographic index, giving the soil-topographic index

$$STI = \ln \frac{a_i}{T_0 \tan(\beta)}. \quad (16)$$

The efficacy of using a threshold index to delineate wetlands was again investigated by [*Merot et al.*, 2003], at six sites across Europe, comparing the *TI*, the *STI* and a newly proposed climato-topographic index;

$$CTI = \ln \frac{a_i \cdot ER}{\tan(\beta)}, \quad (17)$$

where *ER* is the annual effective rainfall depth, the average annual precipitation that is not lost to evapotranspiration. The empirical scaling of the *CTI* allowed a single threshold value to produce reasonable estimates of wetland extent and location at the various, distant and hydrologically distinct catchments.

Following up on their previous work in southern Germany [*Güntner et al.*, 2004] test the ability of several different topographic variables and indices performance in estimating saturated areas, including the *TI*, the *STI*, the *CTI* and a soil-climato-topographic index, as well as different schemes for determining the slope and upstream area. More complex indices provided the most accurate estimates of saturated area and indices with measurement-based transmissivities could be improved upon by the use of transmissivities parameterized to fit observed saturated areas; recalling the the findings of studies using TOPMODEL for runoff estimation in LSMs.

Empirical scaling permits the implicit representation of factors like lateral conductivity, spatial variability in evaporation, recharge and vertical conductivity that are not formally represented in the TOPMODEL framework. Efforts to delineate wetlands using the *TI* indicate that given the goal of estimating saturated or wetland area, parameterization by that value is preferred to any other. Observations show that saturated areas vary on seasonal and inter-annual timescales, while attempts to estimates runoff in LSMs suggest that modeled water content can represent variable saturated areas with the use of the topographic index. A model of wetland area, as a parameterized relationship between modeled water content and regional distributions of the topographic index, is proposed as a synthesis of these lines of inquiry.

Modeling wetland area

A point, *WP*, on the histogram of the topographic index is considered the threshold index of saturation, it is a function of the volumetric soil water of layer six, vwc_6, m^3 water/m^3 pore space, calculated in SiB:

$$WP(t) = \left(1 - vwc_6(t)\right) \cdot m \,. \tag{18}$$

SiB layer six is centered at 1⅓ meters, with a thickness of nearly ½ meter; it is the sixth deepest of ten modeled soil layers representing a 10 meter soil column. The parameter, *m*, relating the water content to the threshold value may be a function of the water content itself, which allows scaling of the range of predicted values, or a constant, in which case the range of predicted wetland areas is implicit.

The parameter m is given as a constant m_o, such that:

$$WP_0 = \left(1 - \overline{vwc_6}\right) \cdot m_0 \tag{19}$$

where WP_0 satisfies:

$$WF_O = \sum_{WP_0}^{N} hist_N\left(TI\right), \tag{20}$$

the requirement being that the mean volumetric soil water of SiB layer six, $\overline{vwc_6}$, give the observed wetland fraction, WF_O, as the sum of the histogram of topographic index from WP_0 through its upper bound, N.

Equations (20) is of the same form as that used to calculate the model wetland fraction, WF, as the volumetric water content changes over time:

$$WF(t) = \sum_{WP(t)}^{N} hist_N\left(TI\right). \tag{21}$$

Three hundred bins were used for the 36,252 points in the DEM representing the 9 km^2 surrounding the WLEF tower, giving ~1% difference in wetland area per bin in the relevant range. The bin size is important not only because it controls the sensitivity of the estimate of wetland area on water content, but also because the shape of the histogram may change when the binning interval is varied, see figure (6). Variation in the sensitivity of the calculation therefore necessitates variation in the functional response.

SiB layer six is used because water contents at this depth generally exhibits smooth response to precipitation events and snowmelt. The water content of shallow soil may rapidly fluctuate in response to precipitation, runoff and evaporation; while the water content of the deepest soil layers may be out of phase with seasonal cycles precipitation.

Also, the depth of the layer precludes freezing at the sites in question. While frozen soils are of great importance to boreal wetlands, which are buttressed by layers of impermeable permafrost, special treatment of this phenomenon may be required in SiB [*Schaefer et al.*, 2009]. Freezing causes particular problems when water contents are used to estimate water table depth based on assumed distributions of soil matric potential, since freezing violates these assumptions [*Clapp and Hornberger*, 1978]. Relating water content to saturated area directly based on empirical parameterization may circumvent this problem.

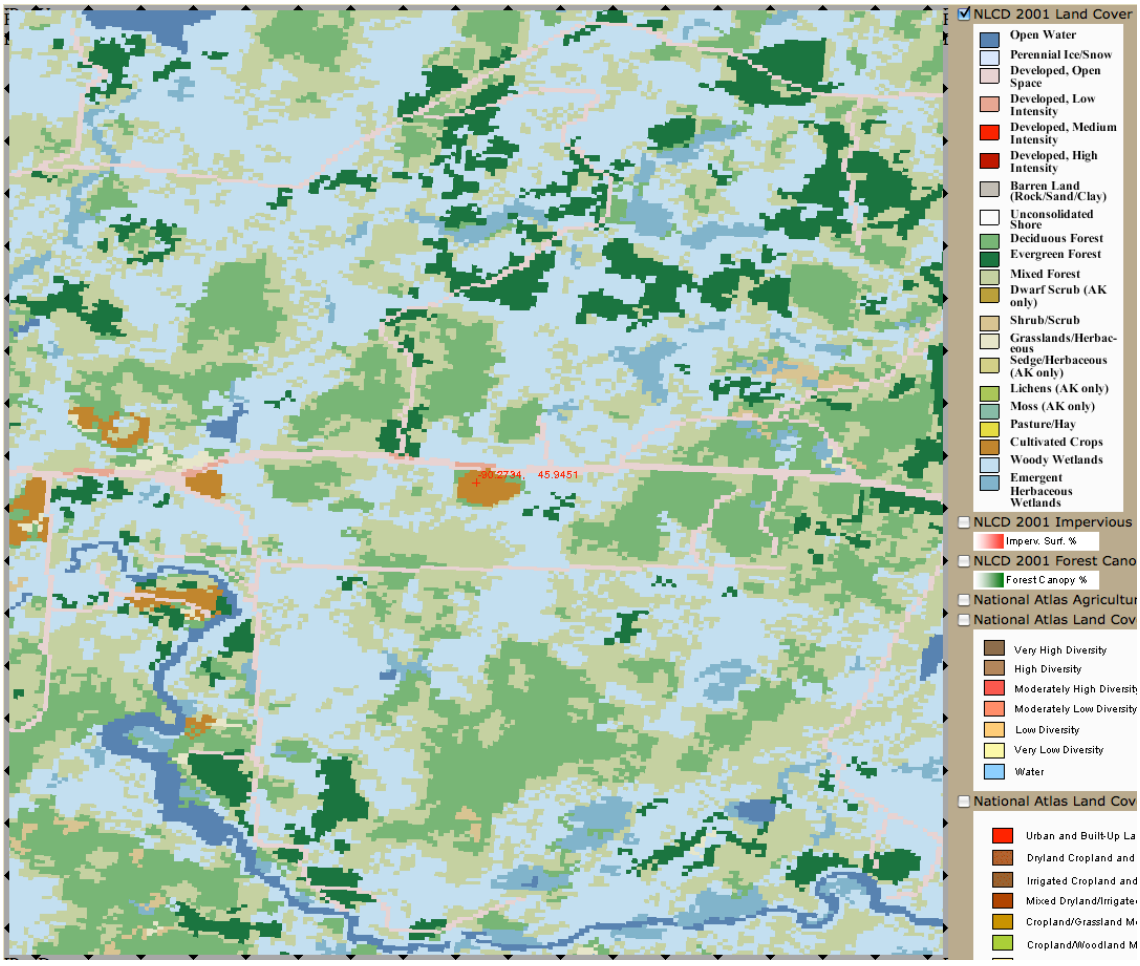

Figure 7: The National Land Cover Database 2001, gridcell length is 30 meters, showing the 9 km^2 region surrounding the WLEF site.

The observed wetland fraction was taken from the 200 meter resolution National Land Cover Database 2001, NLCD, which classified 28.68% of the 9 km^2 region around the WLEF tower as "woody wetland" or "emergent herbaceous wetland" [*Homer et al.*, 2001].

With a constant *m* the range of potential wetland fractions is determined by the range of potential volumetric water contents, the general limits of which are the field capacity, beyond which water must runoff, and the wilting point, below which transpiration ceases. These are calculated in SiB as parameterized functions of the soil, sand and clay fractions determined from USDA maps [*K. Gurney, comment, SiB code*]. At the WLEF site, these limits correspond to wetland areas of 43.69% and 15.8% respectively. Neither of these limits is ever reached in the model runs at the WLEF site, SiB was run over the period from 1997 through 1999, following a ten year spin-up using locally obtained drivers described in [*Baker et al.*, 2003].

Given knowledge of the seasonal variation in wetland extent, *m* could be parameterized as a function of *vwc*, allowing control of the limits of the predicted values as well as the sensitivity of the predicted wetland fraction to the predicted volumetric water content. Further control of the predicted wetland area might also be afforded by an additional parameter, describing the point on the distribution of the *TI* beyond which terrain is considered to be inundated rather than saturated [*Gedney and Cox*, 2003]. However, this approach is less appropriate when unmodified DEMs are used, since the highest values of *TI* tend to be seen in areas of convergence rather then stream channels.

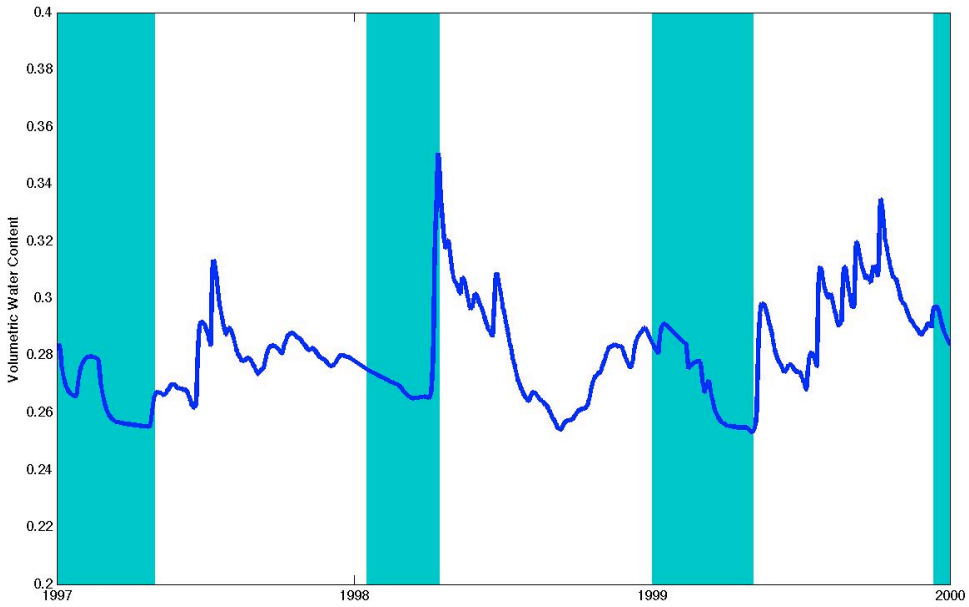

Figure 8: The volumetric water content (m^3_{H2O}/m^3_{layer}) of SiB layer 6 (1.3 meters below the surface) at the WLEF site from 1997 through 1999; shading indicates times when soils were modeled as frozen or near frozen, < 275 K.

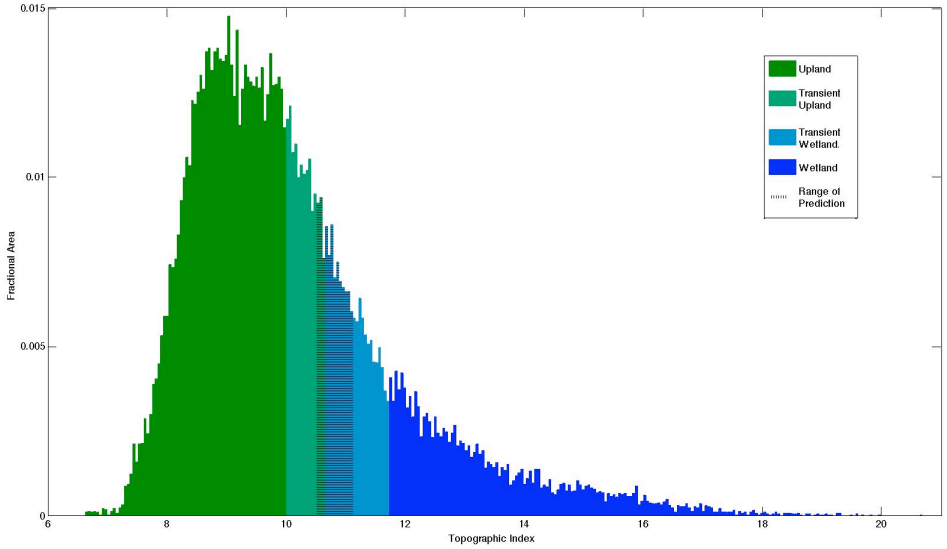

Figure 9: Histogram of the topographic index, frequency normalized to area, of the smoothed 9 km^2 region surrounding the WLEF site with 300 bins. Lighter colors indicate bins capable of inundation or abatement. Shading indicates the range of inundated bins during the three year model run from 1997 through 1999.

It should be emphasized that even in the simple scheme, with *m* as a constant, the relationship between water content and wetland area is not, since the slope of the histogram of topographic index is never or very rarely constant. Histograms of the topographic index are, at the WLEF site and generally normally distributed though skewed toward lower values with a long tail out toward the highest values.

The distribution of volumetric water content at the WLEF site is also skewed toward drier values, which causes a skewed distribution of predicted wetland areas; despite some compensation by the shape of the distribution of the topographic index near the *WP*.

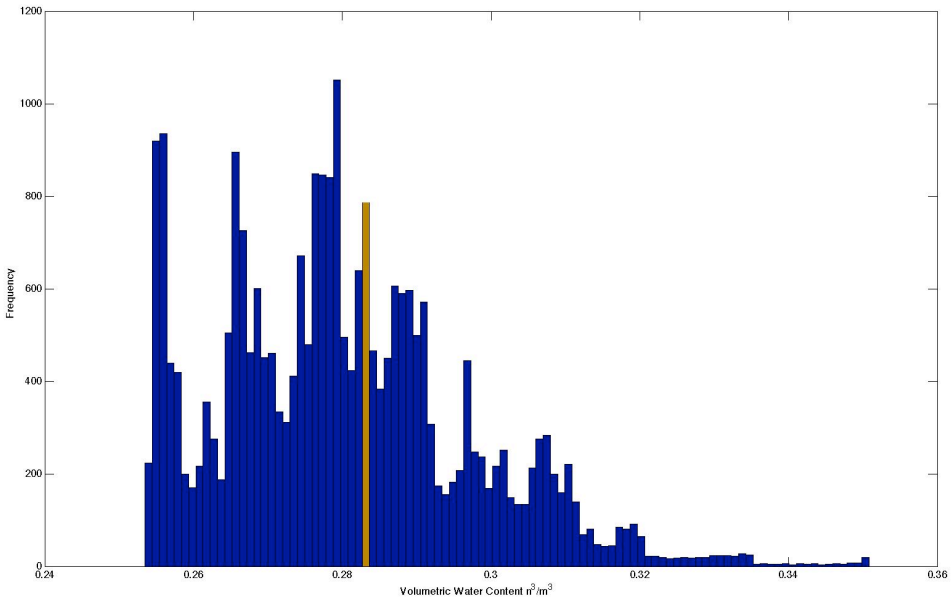

Figure 10: Histogram of the volumetric water content of SiB layer 6. The bin containing the mean value is highlighted.

The choice of *m* such that the mean modeled water content produces the observed wetland fraction is nearly, but not exactly equivalent to the choice of *m* such that the mean modeled wetland fraction is equal to the observed wetland fraction. An average wetland area of 28.73% is predicted rather than the observed 28.68%. This discrepancy results form the sum over the histogram of the *TI*, which makes the relationship of *WF* as a function of vwc_6 non-linear. A solution for *m*, such that the mean predicted wetland area equals the observed wetland fraction is found by iteration with increments of 0.05 *m*. At the WLEF, the resulting value of $m = 122.35$ is very near to the value calculated using the mean water content $m = 122.265$, predicted wetland areas are accordingly similar; such close agreement is not always found at other locations.

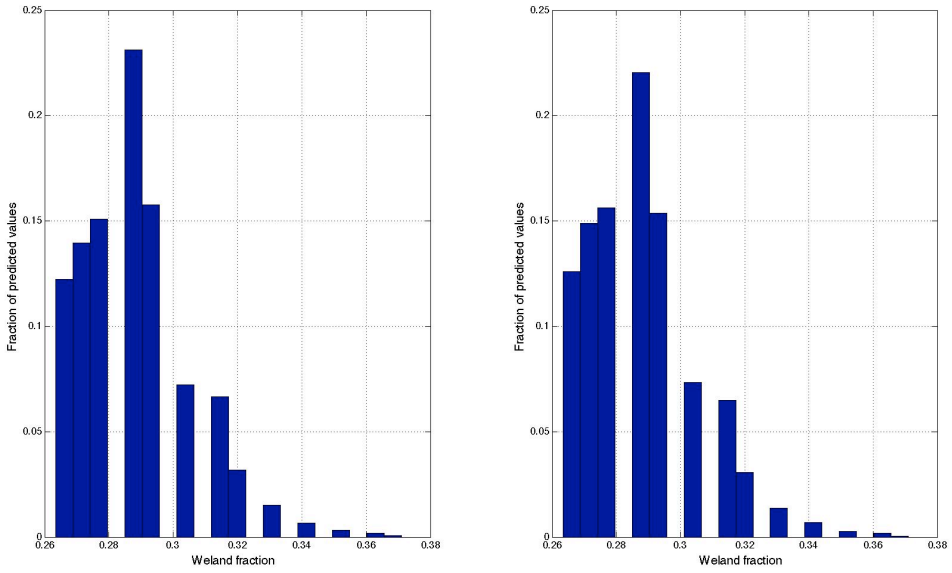

Figure 11: Histograms of predicted wetland area at the WLEF site from 1997 through 1999. Left, using m, such that the average water content gives the observed wetland fraction, right, using m, such that the average predicted wetland area equals the observed wetland fraction.

Lower wetland fractions are more commonly reported when *m* is picked such that the mean predicted wetland fraction equals observed wetland fraction. Varying *m* produces a vertical shift in the curve of predicted wetland area, when a larger number is used, lower wetland fractions are predicted.

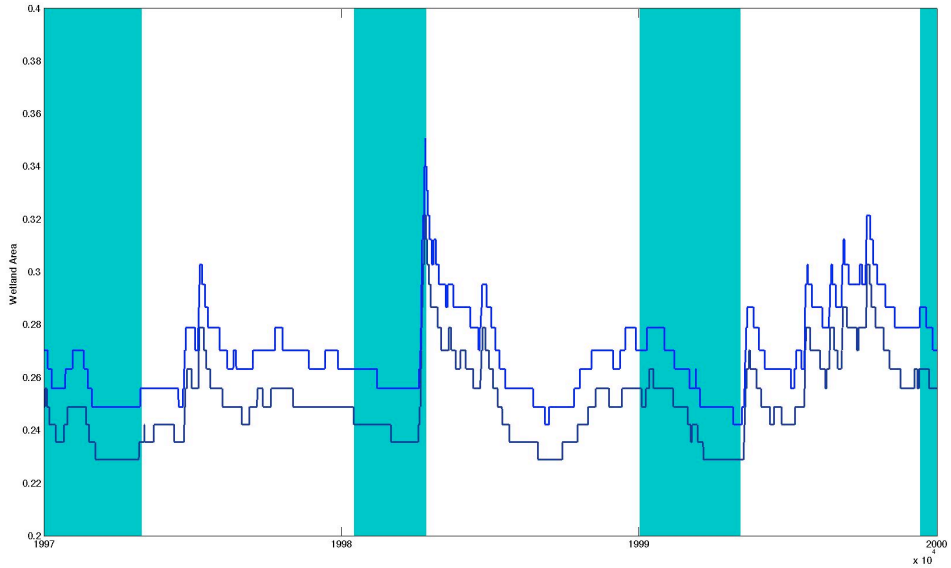

Figure 12: Predicted wetland area at the WLEF site from 1997 through 1999. The upper curve results from requiring the mean water content to give the observed wetland fraction 28.68%, *m = 122.35*. The lower curve from requiring the modal water content to give a wetland fraction of 25%, *m = 129.00*. shading indicates times when soils were modeled as frozen or near frozen, < 275 K.

Assuming a constant value for *m* produces estimates of the wetland fraction that vary within the rage of reported observational estimates. The wetland fraction in the 9 km^2 surrounding the WLEF in the NLCD, derived from arial photography, is 28.68%. Evaluation of imagery from the LANDSAT Thematic Mapper, a satellite, gives an estimate 28% wetland within a 3 km radius of the WLEF-TV tower [*Werner et al.*, 2003]. A detailed survey of the 2.5 km x 3 km area centered at the tower, combining ground

surveys, aircraft observations and satellite imagery, reports 40% forested wetland in the region [*MacKay et al.*, 2002]. A range of predicted variation corresponding to the range of reported values serves in place of direct assessments of the variability of wetland area which would ideally serve for parameterization of m as a function.

The scale dependence of the parameterization of m is investigated by expanding the area of consideration from the 9 km^2 surrounding the WLEF tower to the 1˚ x 1˚ DEM quadrangle containing the tower [*Gesch*, 2007; *Gesch et al.*, 2002]. The topographic index was calculated using the smoothing method developed and described in the first chapter and a 300 bin histogram was created.

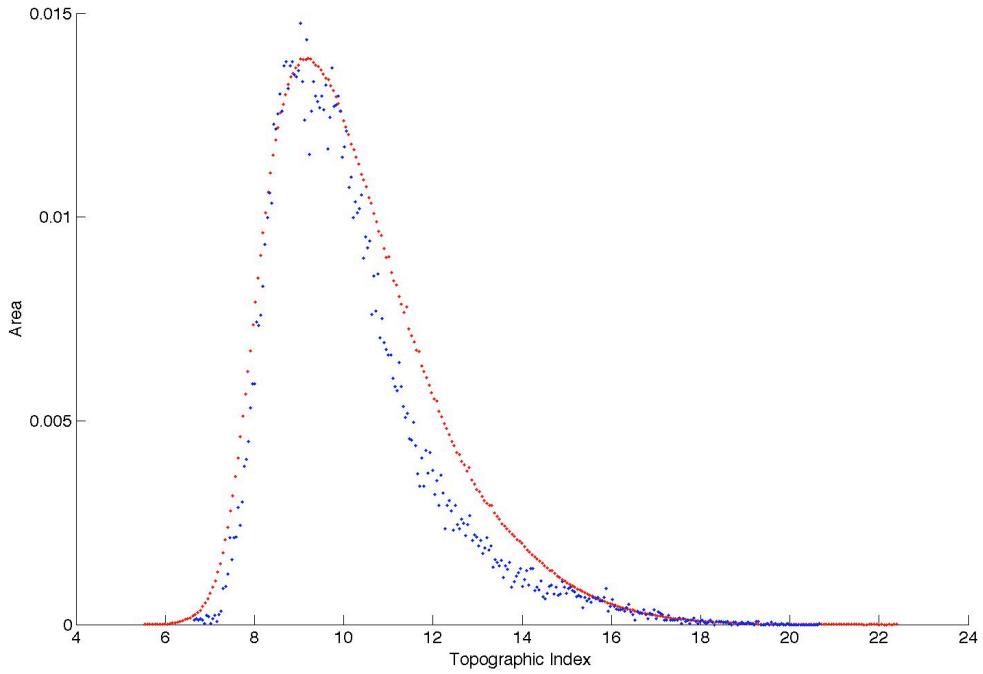

Figure 13: Histograms of the topographic index with 300 bins and frequencies normalized to fractional area. The 9 km^2 region surrounding the WLEF tower in blue, the 1˚ x 1˚ DEM quadrangle containing the tower in red.

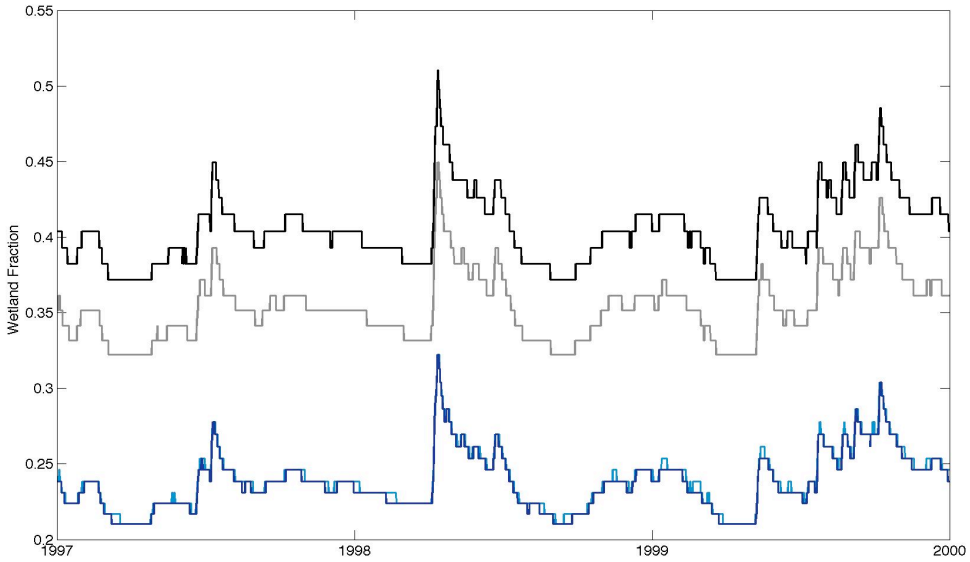

Figure 14: Predicted wetland fractions for the 1˚ x 1˚ quadrangle containing the WLEF site. Values of *m* calibrated in the 9 km^2 surrounding the WLEF tower for $WF_O = 28.86\%$ are used in black and $WF_O = 25\%$ are used in grey. Predictions using the values of *m* calculated for the 1˚ domain, $WF_O = 23.77\%$, are shown in blue. The lighter uses the $m = m_0$ method and darker uses the iterative solution for *m*.

The wetland fraction reported in the NLDC was 23.77% in the larger domain [*Homer et al.*, 2001]. The values of *m* calibrated at the smaller region overestimate wetland area in the larger domain, and produce larger fractions then those they were parameterized for. When *m* is re-calculated for the observed wetland fraction in the larger domain, both methods of calculation of *m* perform well, with seemingly reasonable variability.

Estimates of wetland area are made for to two additional sites, surrounding Tallahassee, FL and Baton Rouge, LA; testing the ability of this method to identify coastal and riverine wetlands respectively. The 1˚ x 1˚ DEM quadrangle containing each city and the corresponding NLCD land cover set were obtained [*Homer et al.*, 2001]

[*Gesch*, 2007; *Gesch et al.*, 2002]. The same methods for calculating the topographic index used previously were applied; water contents were taken from SiB runs at each location over the period from 1993 though 1995, following a spin-up of ten years, with the driver meteorology described in [*Baker et al.*, 2010].

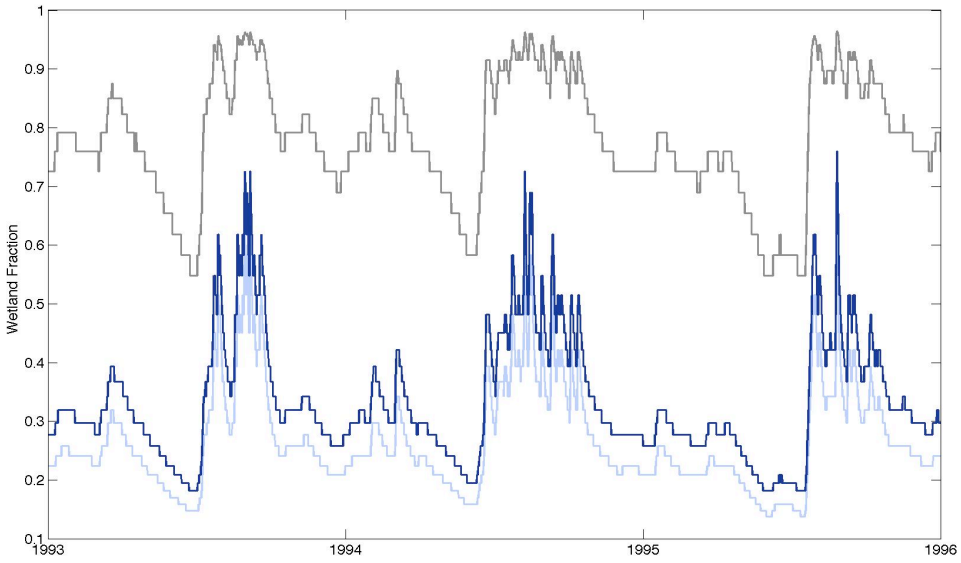

Figure 15: Predicted wetland fractions for the 1˚ x 1˚ quadrangle encompassing Tallahassee, FL. The value of *m* calculated at the 9 km^2 WLEF site for $WF_O = 28.86\%$ is used in grey. The value of *m* calculated locally for $WF_O = 31.87\%$ is used in dark blue. The value of *m* calculated at the 1˚ x 1˚ WLEF quadrangle for $WF_O = 23.77\%$ is used in light blue.

Wetland fractions are overestimated around Tallahassee using the values of *m* parameterized at the 9 km^2 WLEF site. The estimate parameterized in Wisconsin over 1˚ x 1˚ produce more accurate predictions, giving a mean predicted wetland area for the region surrounding Tallahassee of 26.68%, less then the observed fraction of 31.87%, but greater then the 23.77% for which it was parameterized. Using *m* calibrated for the location replicates the observed fraction in the mean, but the estimates are much more

variable than at the WLEF. The magnitude of the range of predicted wetland areas using different constant values of *m* is similar, though the direction and magnitude of the departures from the mean predicted value vary.

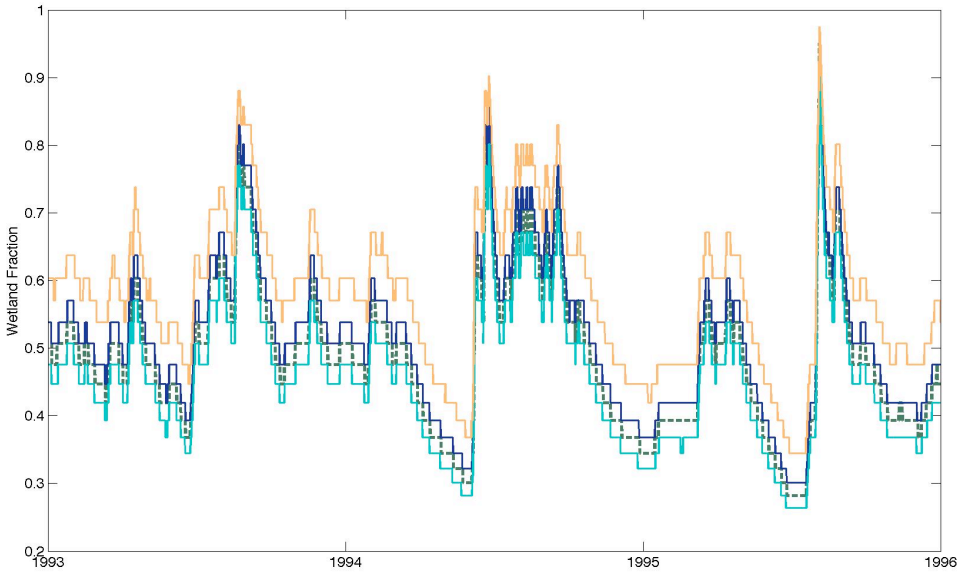

Figure 16: Predicted wetland fractions for the 1˚ x 1˚ quadrangle encompassing Baton Rouge, LA. The value of *m* calculated at the 1˚ x 1˚ WLEF quadrangle for $WF_O = 23.77\%$ is used in the dashed green line. The value of *m* calculated at the 1˚ x 1˚ Tallahassee quadrangle for $WF_O = 31.87\%$ is used in orange. The values of *m* calculated locally for $WF_O = 45.68\%$ are shown in blue; dark blue uses *m* such that the mean water content gives the observed wetland fraction, light blue uses *m* such that the mean predicted wetland fraction equals the observed wetland fraction.

Mean predicted wetland fractions at Baton Rouge are near the observed fraction of 45.68% when values of *m* parameterized over 1˚ x 1˚ domains are used. The parameterization for Wisconsin gives a mean predicted area of 48.62%. The agreement between the Wisconsin parameterized *m* estimates and observed fractions indicates that regional variation in the distribution of *TI* successfully predicts mean wetland extent independently from the parameterization of *m*.

The parameterization for Tallahassee gives a mean predicted area of 58.2%. An overestimate is consistent with the Wisconsin parameterization's underestimate in Florida, suggesting that the Florida region features more wetland than it's topography would generally indicate. This bias may reflect a lack of topographic control over the extent of marine wetlands.

A discrepancy between estimates of wetland area using the different methods of calculating *m* is noticeable at the Louisiana site. Such a departure results from skewed distributions of *TI*, with larger wetland areas predicted when the tail of the distribution extends far out to high values and the mean water content is assigned to the observed wetland fraction.

The magnitude of the variability of the predicted values is again much larger than that seen in the predictions for the WLEF. Parameterization of *m* as a function of the volumetric water content could control this variability, but the range of reported estimates of wetland area at the WLEF is in agreement with the variability of predicted fractions with a constant *m*. Observations of the variability of wetland extent would be necessary to guide parameterization of *m* as a function, and the range of predictions using a constant value for *m* may not be unreasonable.

Reduced variability in estimated of wetland area might be achieved by use of the water content of deeper model soil layers, which exhibit less temporal variability. Distinguishing between saturated and inundated terrain would also limit the range of predicted wetland area, as would schemes distinguishing between saturated area and wetland area on the basis of frequency or duration of saturation.

Simulated and observed fluxes of sensible and latent heat and CO_2

The Simple Biosphere Model was originally proposed by [*Sellers et al.*, 1986] as a land-surface parameterization for general circulation models. As the model was improved upon over time to include more complex ecosystem processes, it became useful as an ecological as well as a meteorological tool [*Denning et al.*, 1996]. SiB represents carbon assimilation by implementation of the photosynthetic enzyme kinetics of [*Farquhar et al.*, 1980] in a model of stomatal conductance based on the Ball-Berry relationship [*Collatz et al.*, 1991]. The model limits photosynthesis based on temperature, relative humidity, soil moisture availability and light availability. Stomatal control of photosynthesis also regulates heat fluxes from plant canopies [*Sellers et al.*, 1996], which allows prognostic calculation of the temperature, moisture and trace gas concentration in the canopy air space [*Vidale and Stöckli*, 2005], and their subsequent exchange with the atmosphere.

A verification of SiB2.5 was performed by [*Baker et al.*, 2003] comparing modeled fluxes of sensible and latent heat and CO_2 to observations made at the WLEF over the three year period from 1997 through 1999. That study found good agreement between model estimates and observations on diurnal, synoptic and seasonal time scales. However, model estimates of the latent heat flux and the net ecosystem exchange were superior to those of sensible heat flux, which was found to be overestimated in the model, particularly in the spring. This bias was presumed to result from errors in the model phenology resulting from the use of monthly maximum NDVI observations to drive model parameters. It was also suggested that wetlands at the site could account for the

discrepancy between modeled fluxes and observations. A run with local drivers, but grassland vegetation and a saturated soil column to simulate wetland conditions, was tiled with the original run in proportions to obtain agreement between model estimated and observed Bowen ratios. An estimate of 35% wetland was found and considered to be in agreement with the estimate of 40% by [*MacKay et al.*, 2002] corroborating the notion that wetlands were responsible for discrepancies between the model and observations.

This work was performed with SiB 2.5, several modifications were made to the model since that time, comprising SiB3 [*Liu*, 2004].

1. The number of soil layers in the model was increased from three to ten.
2. Model treatment of snowpack was considerably revised.
3. Plant roots are now modeled as exponentially declining in density with depth rather than as a single cluster.
4. The function relating soil water to plant stress was redefined.

The changes to the soil column and root structure were found to bring model estimates of NEE in line with observations at the Tapajos field station in Brazil, where previously, the predicted annual cycle of net ecosystem exchange had been reversed [*Baker et al.*, 2008]. This is a considerable improvement and a striking finding, but these changes, an improvement in the tropics, have had unintended consequences at the WLEF.

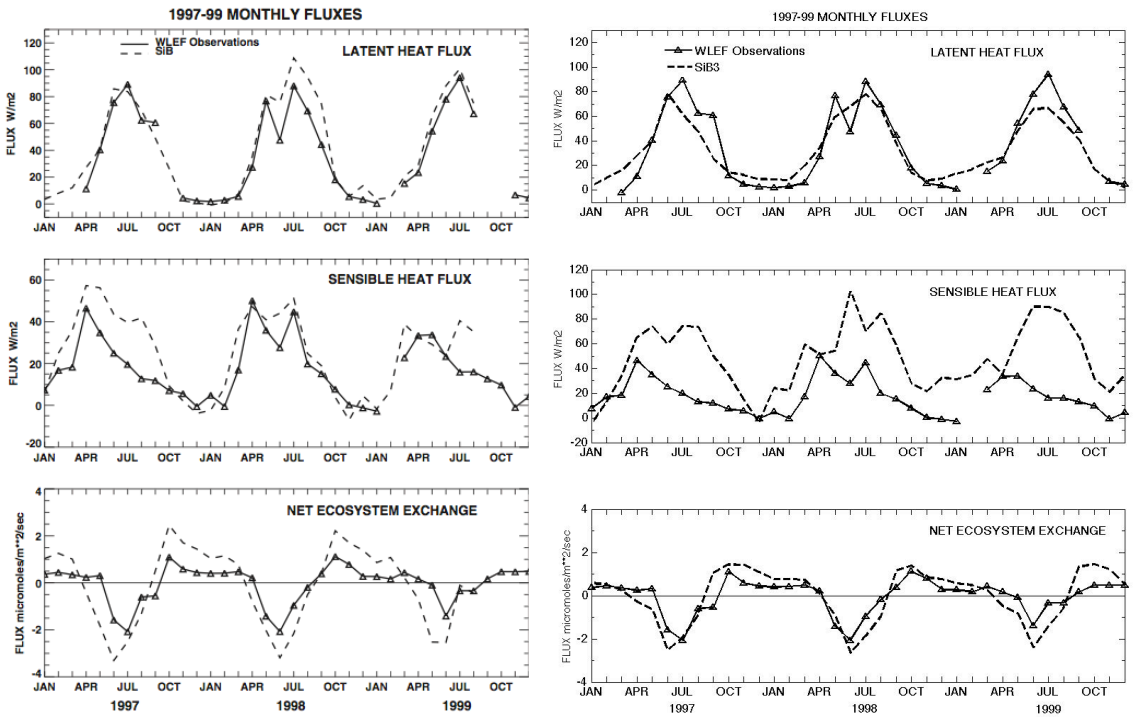

Figure 17: Modeled and observed sensible and latent heat fluxes and net ecosystem exchange at the WLEF site. On the left, model estimates from SiB2.5, reproduced from [*Baker et al.*, 2003]. On the right, model estimates from SiB3.

Previously, close agreement between modeled and observed latent heat fluxes was found, the new model configuration has introduced errors. Not simply a shift; wintertime fluxes, formerly in close agreement, are now overestimated and summertime fluxes, formerly slightly overestimated, are now underestimated. Sensible heat fluxes, previously seen to be somewhat overestimated in the springtime, now show considerable overestimates year round. On the other hand, predictions net ecosystem exchange has improved, with reduction in both the positive wintertime bias and the negative summertime bias seen in SiB2.5.

These changes imply that plants are experiencing water stress in SiB3, but were not in the older version of the model. The equation relating the water content to water

stress in SiB2.5 resembles a step function, with stress increasing very rapidly as water content approaches the wilt point. In SiB3, a new relationship was defined, more closely resembling a logistic curve. The new parameterization eases stress on plants when water content is near the wilt point, but increases stress on plants at some water contents further from the wilt point, at values that had previously been on the unstressed side of the step function. This explanation is consistent with the observed changes in summertime, more stress causes stomates to close, reducing latent heat flux and increasing sensible heat flux while limiting CO_2 uptake. The increases in modeled wintertime heat fluxes may result from the changes to the treatment of snow-cover and increased heat storage in the thicker soil column, energy balance is maintained.

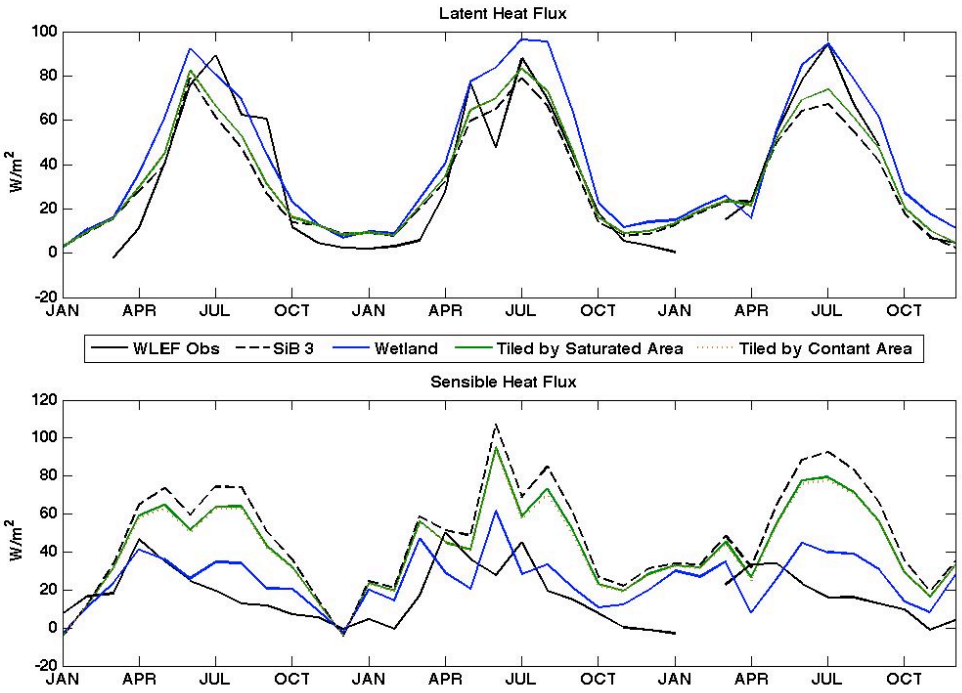

Figure 18: Latent and sensible heat fluxes at the WLEF site.

Analysis of the impact of wetlands at the site in SiB3 analogous to the analysis performed with SiB2.5 is attempted. But, as predictions from SiB are no longer in such close agreement with the observations at the WLEF site, tiling to correct the Bowen ratio no longer produces a reasonable estimate of wetland area. Now, in fact, close correspondence is seen between the observations and heat fluxes estimated in the "wetland" run, indicating a wetland area of 100%.

Tiling affords some improvements, but these are overwhelmed by the errors in the initial estimates. Tiling by predicted wetland fraction is nearly indistinguishable from tiling by the constant wetland area reported in the NLCD. This indicates that the variably modeled wetland fraction did not aid estimates, but given the magnitude of the predicted variability close agreement is to be expected at the WLEF site that may not be found elsewhere. Furthermore, the size of the error in the initial estimates suggests dismissal of the approach on these grounds is premature.

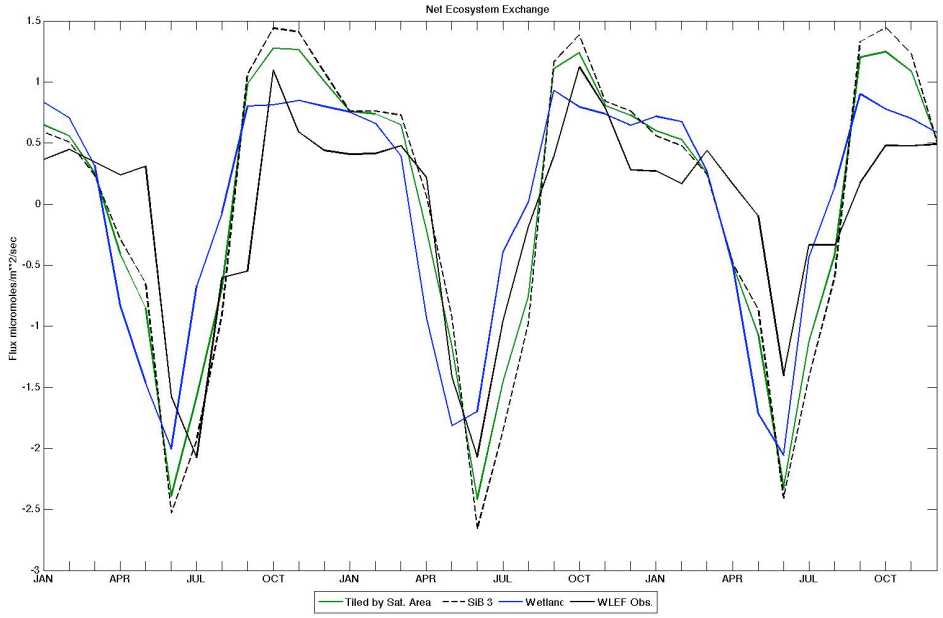

Figure 19: Net ecosystem exchange at the WLEF site.

Modeled net ecosystem exchange shows improvement with tiling beyond the improvement seen in the switch to SiB3. Summertime drawdown is brought closer to the observations as is wintertime efflux, however the general biases do remain. Rarely, tiling actually hurt estimates as in April and May of 1997 and February and March of 1999. Estimates of wetland area based on the tiling NEE were erratic, even with monthly averages. Excluding outliers, an average wetland area of 31% brought predicted NEE in accordance with observations. This estimate could serve as target for scaling m, but uncertainties are too large to guide parameterization of m as a function of vwc_6.

3. METHANE

Atmospheric methane

Global average atmospheric methane concentrations of 1790 p.p.b. in 2008 [*Dlugokencky et al.*, 2009] exceed a doubling of pre-industrial concentrations of 700 ±30 p.p.b., as determined from ice cores [*Rasmussen and Khalil*, 1984]. The gas has an average atmospheric lifetime of 8.4 years with the primary sink, oxidation to carbon dioxide by the hydroxyl radical, ten times greater than the sinks from methanotrophic consumption in soils and oxidation to water vapor in the stratosphere [*Cicerone and Oremland*, 1988; *IPCC*, 2007; *Lelieveld et al.*, 1998]. Wetlands are the dominant natural source of the methane to the atmosphere, accounting for 20% of the global flux in a "bottom-up" accounting [*Wuebbles and Hayhoe*, 2002] and 40% in one inverse modeling study [*Mikaloff Fletcher et al.*, 2004]. This flux is, in most accounts, eight times larger than the next largest natural flux, emissions from enteric fermentation in the digestive systems of termites; with all other natural sources nearly negligible [*IPCC*, 2007]. Classifications of anthropogenic methane sources show roughly equal contributions to the total flux, and include enteric fermentation from ruminant livestock, emissions from

landfills, coal mining, oil & gas exploration, biomass burning and rice agriculture [*IPCC*, 2007].

Despite the long-term increase in atmospheric methane concentrations, little or no increase was seen from 1999 through 2006, [*Rigby et al.*, 2008], leading to speculation about arrival at a new atmospheric steady-state concentration in an anthropogenically perturbed regime [*Dlugokencky et al.*, 2003]. This theory was bolstered by modeled indication of stabilization of anthropogenic emissions of methane from incomplete combustion and fossil fuel extraction in the preceding decade [*Dlugokencky et al.*, 1998]. However, measurements of ethane concentrations, which shares common fossil-fuel sources with methane, indicate that these emissions leveled off in the decade preceding that [*Aydin et al.*, 2011], and the methane trend may be more consistent with reductions in sources from biomass burning [*Simpson et al.*, 2006]. Isotopic ratios of $^{13}C/^{12}C$ in atmospheric methane indicate that leveling of the gas's growth rate is consistent with decreasing microbial sources rather than decreased fossil fuel emissions [*Kai et al.*, 2011], a pattern consistent with an earlier inverse modeling study [*Bousquet et al.*, 2006] and with predictions of decreasing emissions from rice agriculture due to changing agricultural practices [*Li et al.*, 2002].

Warm arctic temperatures have been suggested as an explanation for the return to rising atmospheric concentrations after 2006 [*Dlugokencky et al.*, 2009], as has decreasing hydroxyl concentrations [*Rigby et al.*, 2008]. The magnitude of seasonal and intra-seasonal variations in atmospheric hydroxyl concentrations is a subject of some debate. [*Manning et al.*, 2005] report frequent anomalies on the order of 10% using ^{14}CO

as a diagnostic. Variability as high as 25% was also seen by [*Bousquet et al.*, 2005] and [*Prinn et al.*, 2005] using methyl chloroform as a diagnostic, but much less frequently. [*Montzka et al.*, 2011] argue that most of the variability found in those studies results from uncertainty in methyl chloroform emissions and errors relating to large spatial gradients in its concentration. They suggest that as concentrations of methyl chloroform decline, following its ban in the Montreal Protocol, estimates in OH variability using the gas should improve, and point to more recent estimates of variability on the order of 5% as more accurate.

Finding conflicting explanations for the observed trends in atmospheric methane concentrations among "top-down" inverse modeling and regional box-model studies suggests that better "bottom-up" prior estimates are needed. Using observations of wetland area to scale estimates of wetland methane emissions [*Ringeval et al.*, 2010] found that wetland area accounted for 30% of the inter-annual variation in boreal wetlands and 40% and 60% of the seasonal variation in temperate and tropical emissions. Modeled estimates of wetland should therefore be a useful if not critical component of a model of wetland methane emission.

Methanogenesis and methanotrophy

The diffusion rate of oxygen through saturated soils is sufficiently slow that the molecule is depleted in wetland soils by heterotrophic microbial respiration of organic carbon within hours of inundation [*Mitsch and Gosselink*, 2007]. Lacking O_2 as an electron acceptor, microbial respiration shifts to the reduction of nitrate, a less energetic

substrate. Nitrate also eventually depletes and respiration moves though catabolic pathways at progressively lower redox potentials, Mn^{4+} and Fe^{3+} are reduced if available, followed by sulfate before the system enters the methanogenic regime.

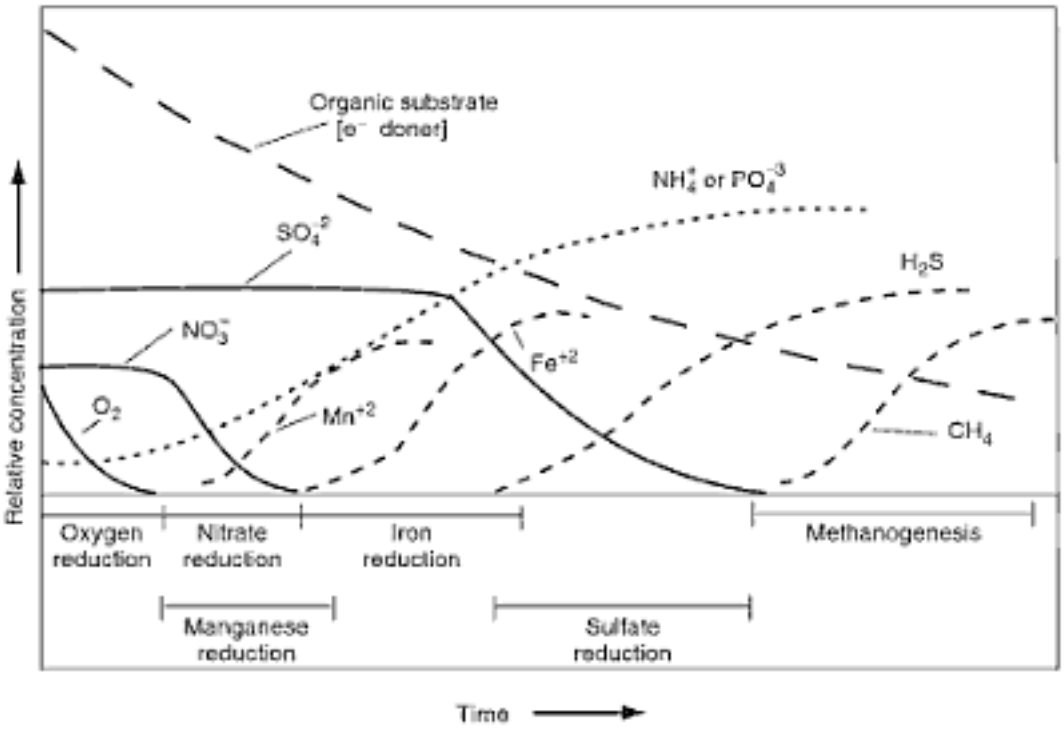

Figure 20: Sequence of reduction pathways and relative concentrations of electron acceptors and respiratory products. Reproduced from [*Mitsch and Gosselink*, 2007].

There are three types of substrate used by methanogens to generate energy:

1. H_2 / CO_2, CO, or formate ($CHOO^-$),

2. methanol (CH_3OH), and other methylated compounds,

3. acetate (CH_3COO^-).

These substrates are respiratory products of hydrolytic, fermentative and acetogenic bacteria which consume sugars, amino acids and fatty acids derived from plant material [*Reddy and DeLaune*, 2008]. Methanogens are therefore dependent on these bacterial communities for their survival. However, the dependence is often mutual, some

acetogens form a syntrophic relationship with methanogens [*Reay et al.*, 2010]. Acetogens' utilization of certain compounds, such as propionate, are energetically favorable only at very low H_2 concentrations, but H_2 is generated in their consumption of propionate, see table (2). Only with methanogens present to consume the produced H_2, as well as the acetate and CO_2, can the reaction proceed.

Table 2: Example catabolic reactions

Methanogenic		ΔG° [kJ]
$4H_2 + CO_2$	➔ $CH_4 + 2H_2O$	-131
4 $formate^- + 4H^+$	➔ $CH_4 + 3CO_2 + 2H_2O$	-145
$4CO + 2H_2O$	➔ $CH_4 + 3CO_2$	-211
$Acetate^- + H^+$	➔ $CH_4 + CO_2$	-36
4 methanol	➔ $3CH4 + CO_2 + 2H_2O$	-106
H_2 + methanol	➔ $CH_4 + H_2O$	-113
$4H_2 + HCO_3^- + H^+$	➔ $CH_4 + 3H_2O$	-136
Acetogenic		
Glucose + H_2O	➔ 2 $acetate^- + 2HCO_3^- + 8H_2$	-207
$Propionate^- + 2H_2O$	➔ $Acetate^- + CO_2 + 3H_2$	+72, P_{H2} = 1Pa -21, P_{H2} < 1Pa

[*Reay et al.*, 2010; *Reddy and DeLaune*, 2008]

At landscape scales, methanogenesis, like more commonplace respiratory pathways, are usually modeled as a temperature dependent chemical reaction using Arrhenius-type or van 't Hoff equations [*Bohn et al.*, 2007; *Cao et al.*, 1996; *Davidson et al.*, 2006; *Eliseev et al.*, 2008; *Gedney et al.*, 2004; *Potter et al.*, 2006; *Walter et al.*, 1996;

Zhang et al., 2002; *Zhuang et al.*, 2004]. These functions are often additionally scaled by water table height, sometimes by labile carbon availability, [*Cui et al.*, 2005], or by CO_2 respiration, [*Potter*, 1997], and more rarely by pH and redox potential [*Cao et al.*, 1998] since these factors are difficult to assess over large areas. Water table depth is considered the greatest limiting factor to methanogenesis, as methanogens are strict anaerobes [*Walter et al.*, 2001].

Within the context of a column-structured ecosystem model like SiB, regulating methanogenesis by water table depth and regulating by wetland area are functionally equivalent. One assumes in either case that modeled value is representative of a distribution of different water table depths within the modeled area. Thinking in terms of water table depth is more amenable to modeling subsurface gas transport, which this model does not consider. Wetland area follows more clearly from the use of spatial topographic information, which may better inform estimates. The difference is conceptual and the methods developed for predicting wetland area in chapter two may easily be adapted to frameworks dealing with water table depth, for instance, by inverting the logic in TOPMODEL, equation (15).

Estimated wetland fractions follow the methods outlined in chapter two. The focus is again on the WLEF site, with *m* calculated such that the mean predicted wetland area equaled the observed wetland area. An observed wetland area of 25% is assumed, lower than the observed wetland area from the NLDC, see figure (12).

Methanogenesis is modeled as a temperature dependent reaction, scaled by the wetland fraction:

$$CH_4 production = WF \cdot Q_{10P}^{\left(\frac{td_6 - 273.15}{10}\right)}, \quad (22)$$

where Q_{10P} is the factor by which methanogenic respiration is multiplied with every 10˚ temperature increase. [*Whalen*, 2005] reviews twelve studies estimating Q_{10P} *in situ* in different wetland environments and reports an astounding variation; reported values ranged from 1 to 35 in one study while estimates from 1.2 to ~8 were common from the others. Considerable variation is also found in laboratory-based measurements. Another review, [*Segers*, 1998], presents results from14 studies finding Q_{10P} values ranging between 1.5-28 in soil samples, and results from eight studies finding Q_{10P} values ranging between 1.3 and 12.3 in pure cultures. A value of 6 was chosen for most of this analysis and this parameter space is explored.

Methanotrophy is modeled by a similar equation to occur only in the upland fraction [*von Fischer and Hedin*, 2007]:

$$CH_4 consumption = (1 - WF) \cdot Q_{10C}^{\left(\frac{td_6 - 273.15}{10}\right)}, \quad (23)$$

where Q_{10C} is the factor by which methanotrophic respiration is multiplied with every 10˚ temperature increase. Estimates for this value are in closer agreement then for Q_{10P}, four studies found values ranging from 1.8 to 2.9 [*Whalen*, 2005]. A value of 2.4 was used in this study. Temperatures for each reaction are taken from SiB soil layer six, td_6, see figure (21) and the description of equation (16).

Methanotrophy is not limited by methane availability. This decision is motivated by an interest in the essential interactions of inversely proportionally scaled reaction rates, the problem of incorporating non-local contributions to methane concentrations and the fact that subsurface transport mechanisms are neglected.

Methane flux from the ground to the model canopy air space is simply the balance between methanogenesis and methanotrophy plus *k,*

$$CH_4 flux = CH_4 production - CH_4 consumption + k\,, \tag{24}$$

where *k* is a constant and may be considered a baseline production of methane. Not shown is an additional constant scaling factor used to bring the arbitrary units of the prediction into mol/m^2.

For a given temperature and value of *k* there is a critical wetland fraction at which methane production will equal methane emission and the flux will be zero,

$$WF_{Crit} \cdot Q_{10P}^{\left(\frac{td_6 - 273.15}{10}\right)} + k = \left(1 - WF_{Crit}\right) \cdot Q_{10C}^{\left(\frac{td_6 - 273.15}{10}\right)}. \tag{25}$$

By choosing $k = k_0$, such that equation (25) is satisfied when the critical wetland fraction is equal to the observed wetland fraction, $WF_{Crit} = WF_O$, at average SiB layer six temperatures,

$$k_0 = \left(1 - WF_O\right) \cdot Q_{10C}^{\left(\frac{\overline{td_6} - 273.15}{10}\right)} - WF_O \cdot Q_{10P}^{\left(\frac{\overline{td_6} - 273.15}{10}\right)}, \tag{26}$$

the requirement that the site be in long-term equilibrium neither a net producer nor consumer of methane is made. This condition is an approximation due to the use of the average temperature, and because covariation between temperature and wetland fraction

will drive the estimates away from equilibrium. This guess serves as a starting point and is the logical place to begin parameterization given adequate measurements of methane flux and wetland area and confidence in the value of Q_{10P}.

With consideration of equations (22), (23), (24) and the seasonal cycle of precipitation and therefore wetland fraction, see figure (12), the basic behavior of the seasonal cycle of methane flux may be inferred. Emission is expected in the summertime as high temperatures coincide with high wetland fractions, conditions favorable to methanogenesis. Consumption is expected in the spring and fall as temperatures are warm, but the region is dry and methanotrophy will dominate. Wintertime fluxes should be near zero as temperatures are too low for either type of respiration.

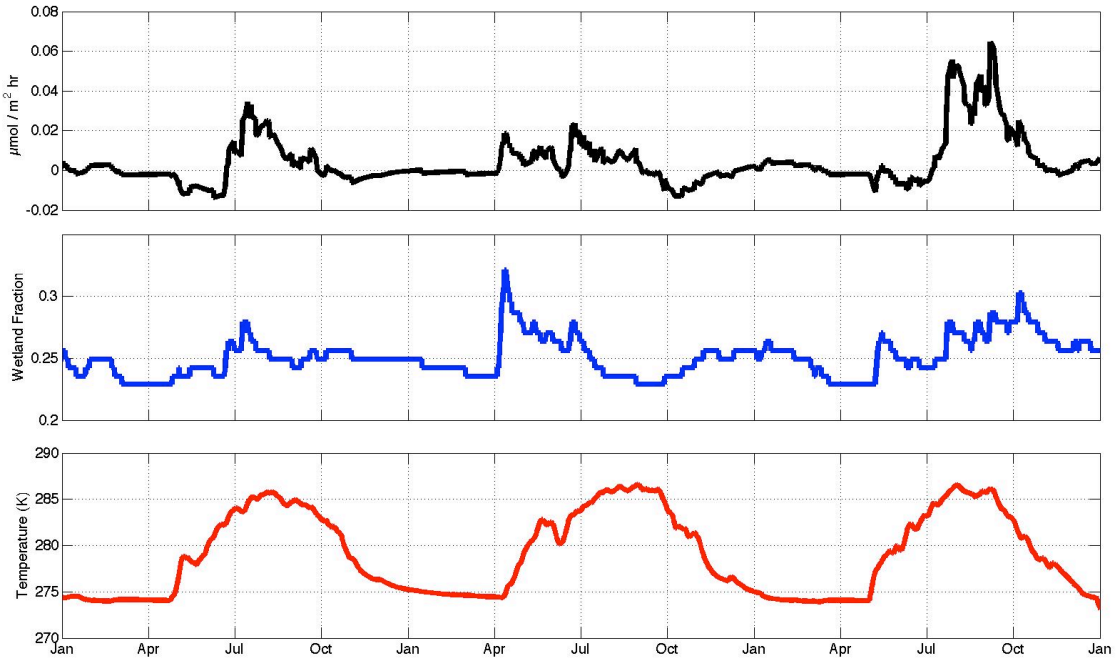

Figure 21: Predicted hourly methane flux, wetland fraction and temperature at the WLEF site over the three year period from 1997 though 1999.

The model behaves as expected with the wetland fraction controlling the basic seasonal cycle of methane flux and the temperature largely controlling the magnitude of the response to variations in the wetland fraction.

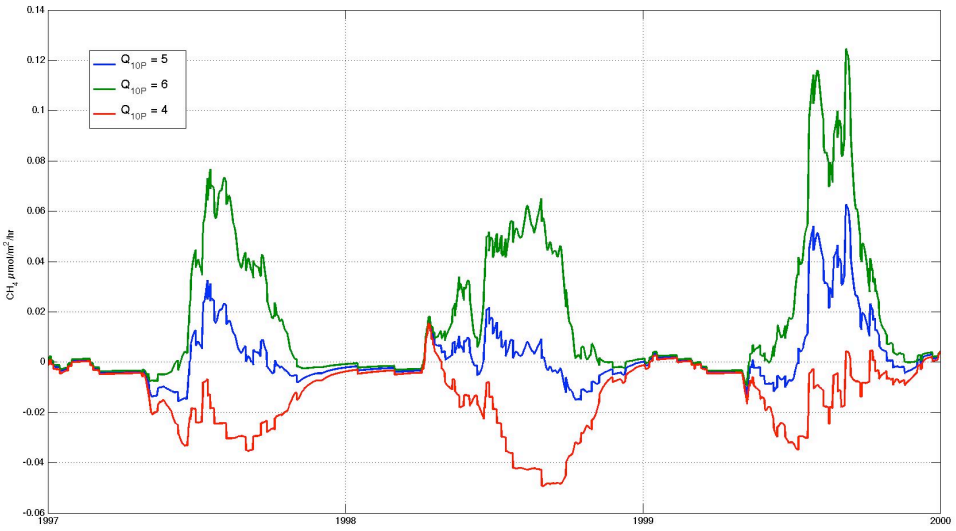

Figure 22: Predicted hourly methane fluxes with variation of Q_{10P} and k held constant.

Variation of Q_{10P} has a substantial impact on model estimates. With a lower Q_{10P}, methanotrophy dominates year round, because of the scaling by WF, even though Q_{10P} remains larger than Q_{10C}. Higher Q_{10P} values predict more methane production in summertime and allows the methanogenic term to dominate at lower wetland fractions in the fall and spring.

Changing Q_{10P} while leaving $k = k_0$ as previously defined means that the site is moved from long-term equilibrium. If k_0 is redefined in equation (26) with the new values of Q_{10P}, this equilibrium is restored.

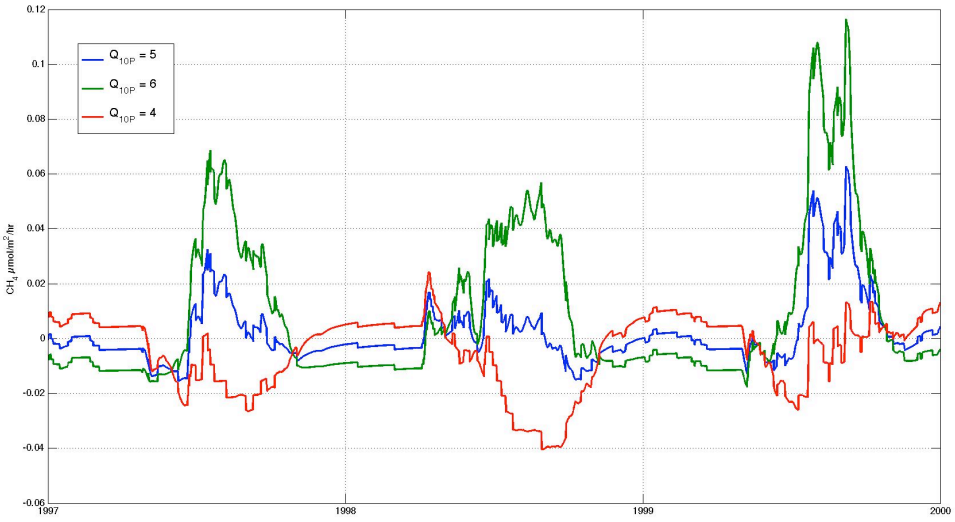

Figure 23: Predicted hourly methane fluxes with variation of Q_{10P} and k redefined to maintain the condition of long-term equilibrium.

Varying k produces a vertical shift in the predictions. Consequently, the predictions move away from the expectation of near zero flux in the wintertime. The long-term equilibrium requirement, when calculated for $Q_{10P}=5$, produces an estimate of the baseline methane production that results in near zero wintertime flux even when other values of Q_{10P} are used to calculate that flux.

The requirement that wintertime flux be near zero may be made by means similar to those for requiring long-term equilibrium. Methane production must equal methane production at average wintertime temperatures and wetland fractions:

$$\overline{WF_W}\cdot Q_{10P}^{\left(\frac{\overline{td_{6W}}-273.15}{10}\right)}+k_W=\left(1-\overline{WF_W}\right)\cdot Q_{10C}^{\left(\frac{\overline{td_{6W}}-273.15}{10}\right)}. \qquad (27)$$

By rearranging equation (27) to solve for k_w, setting $k_w = k_0$ and combining with equation (26), unique solutions for Q_{10P} and k may be obtained that satisfy both the

condition that wintertime fluxes be near zero and the condition that the site be in long-term equilibrium. These two constraints therefore provide a theoretical bases for determining Q_{10P}, given the many assumptions made; not only the accuracy of the constrains, but also that Q_{10C} is known, that temperature and wetland area do not covary and the very structure of the model.

Pairs of Q_{10P} and k_0 that satisfy the long-term equilibrium condition and pairs Q_{10P} and k_w that satisfy the wintertime condition are determined iteratively, the conditions are both satisfied at the intersection of the curves.

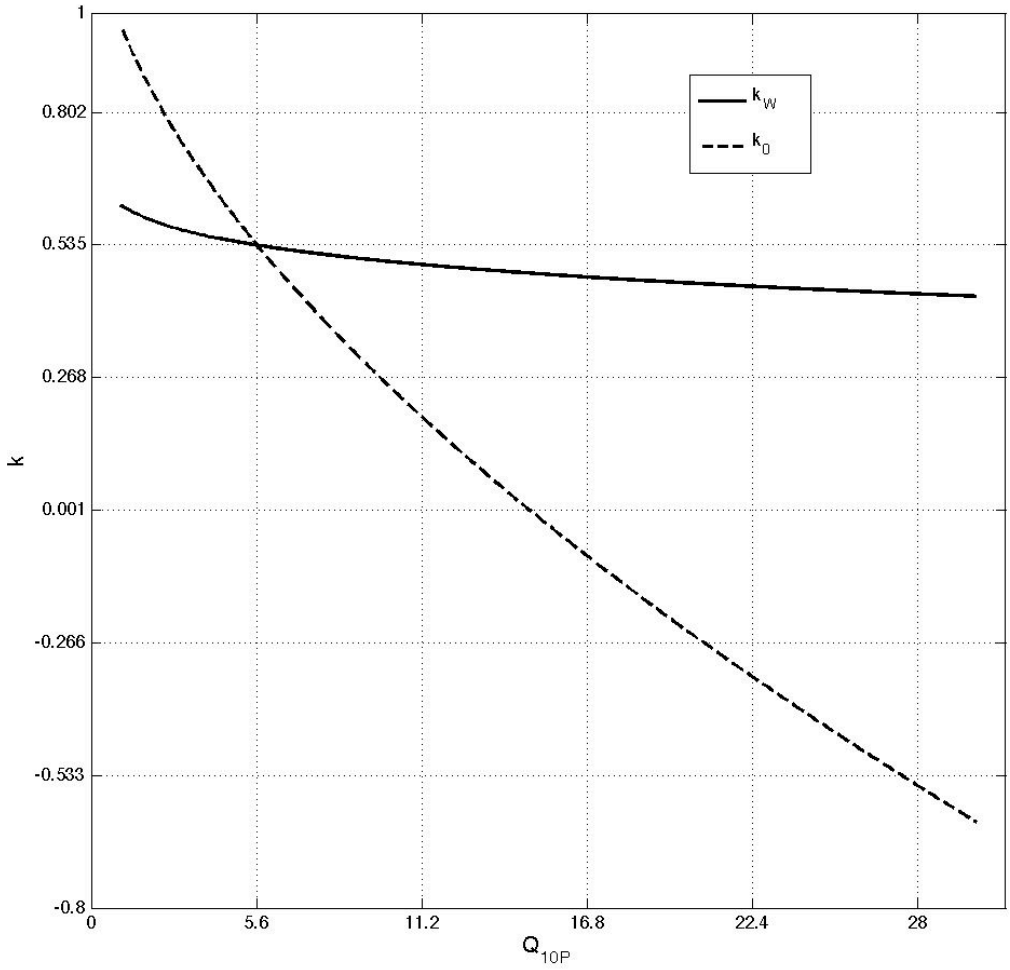

Figure 24: Solutions of k_0, equation (26), and k_w, equation (27), for varying values of Q_{10P}. Both equilibrium conditions are satisfied at the intersect of the curves.

The intersect is seen at $k = 0.535$ and $Q_{10P} = 5.6$, similar to the values initially used, by chance, where $k = 0.5313$ was used as calculated to meet the long-term equilibrium condition for the assumed $Q_{10P} = 5$. There is only slight error with the iterative method and inspection, a $Q_{10P} = 5.6$ produces calculated estimates of $k_0 = 0.5345$ and $k_w = 0.5361$. This suggests that a slightly higher Q_{10P} is appropriate, and may motivate formulation of the analytic solution.

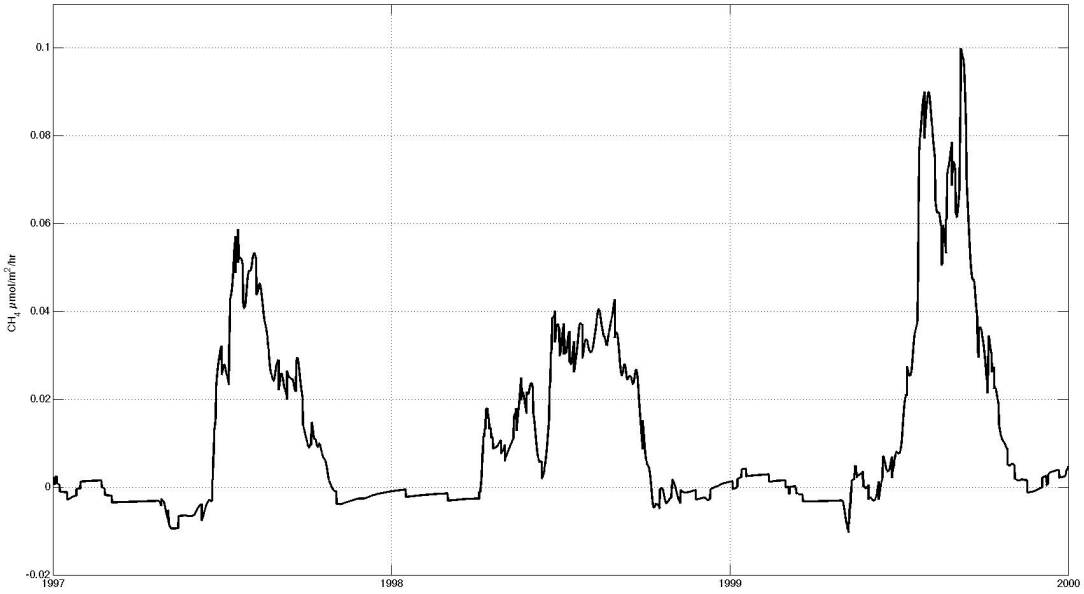

Figure 25: Estimated methane flux calculated with $k = 0.535$ and $Q_{10P} = 5.6$, satisfying the wintertime and long-term equilibrium conditions at the WLEF site over the period from 1997 through 1999.

Use of a higher Q_{10P} value raises summertime peaks in the estimated flux, and the higher k keeps wintertime values close to zero. The seasonal cycle continues to resemble expectations, though the fall and spring drawdowns are diminished compared to the earlier estimates.

The overall effect of raising k and Q_{10P} to meet the two equilibrium conditions is to increase the total methane flux over the modeled period. The zero wintertime flux requirement brings the model further from the assumption of zero net emission, then does raising the Q_{10P} to 6 without adjusting k. A net emission over the three year modeling period of 604 μmol/m^2 is seen with the two equilibrium conditions, compared to a net emission of 453 μmol/m^2 with only the long-term equilibrium condition and the higher Q_{10P}. The use of a higher Q_{10P} exacerbates the effects of covariation between temperature and wetland area in both cases. The long-term equilibrium requirement with the assumption of $Q_{10P} = 5$ produces a substantially smaller net emission of 52 μmol/m^2 over the modeled period.

Given the uncertainty in estimates of Q_{10P}, the potential theoretical constraint given by the long-term and wintertime equilibrium requirements is attractive. But, given the approximations made in the requirements, their unlikely accuracy and the simplicity of the model; the constraint is itself poorly constrained. Still, this analysis may inform comparison of modeled and observed fluxes.

Simulated and observed methane exchange

In wetlands, methane flux is most commonly measured using closed chambers, usually styrofoam or plastic containers clamped to supports embedded in the soil below the water table or driven into the ground. These chambers enclose some area of wetland soil as well as the associated vegetation; this is possible given the usual height of the herbaceous plants typical to most wetlands. Air samples are taken from the chambers

over time and their composition is measured. The technique is mildly disruptive and of limited spatial and temporal scale, but is practical given the low atmospheric concentrations of methane and the variability in the flux of the gas [*Wille et al.*, 2008].

Eddy covariance measurements offer a non-disruptive and high temporal resolution alternative. Studies using this method have been conducted over periods of weeks in north-eastern Greenland [*Friborg et al.*, 2000], northern Finland [*Hargreaves et al.*, 2001], and north-eastern Siberia [*Sachs et al.*, 2010; *Wille et al.*, 2008]; and more recently over seasonal periods in southern Finland [*Rinne et al.*, 2007], north-central Alberta [*Long et al.*, 2010]. Scaling between eddy covariance and chamber methods was investigated by experiment in [*Sachs et al.*, 2010], finding that the large spatial and temporal variations in chamber measurements of methane flux could be upscaled to reflect the larger-scale eddy covariance measurements by weighting chamber fluxes by vegetation type, determined from high resolution, <1 meter, classification from arial photography.

The sampling footprint of eddy covariance measurements, commonly 4-10 km, allows sampling over a wide enough region that the measurement can be considered representative of regions large enough to be appropriate for guiding a model like SiB. This is particularly important with regard to methane, since it exhibits considerable spatial variation in its flux and upscaling chamber measurements is generally impractical.

Eddy covariance measurements of methane at the WLEF site are not yet available, though they have begun, [*A. Desi, personal communication, December, 2010*]. However, comparable estimates of the flux of methane have been made at the site by [*Werner et al.*,

2003] from 1997 though 1999. These estimates use the modified Bowen ratio (MBR) approach, which relates concentration measurements to fluxes. Hourly measurements of methane and carbon dioxide concentration were made at two heights, 30 and 76 meters. The difference between the concentrations of each gas at each height is assumed representative of the vertical gradient of each gas. The methane flux will equal the ratio of the methane and carbon dioxide gradients multiplied by the hourly averaged flux of carbon dioxide as measured by eddy covariance if it is assumed that the transfer coefficients of each gas are the same and equal to the flux of carbon dioxide:

$$Flux_{CH_4-30m} = Flux_{CO_2-30m}\left(\frac{\delta CH_4 / \delta z}{\delta CO_2 / \delta z}\right). \quad (28)$$

Measurement precision was reported as 10 ppb for methane and 0.01 ppm for carbon dioxide. Uncertainty in the carbon dioxide flux measurement was given as <15-40%, with additional uncertainty from the assumption of equivalent transfer rates and the low, hourly, sampling rate.

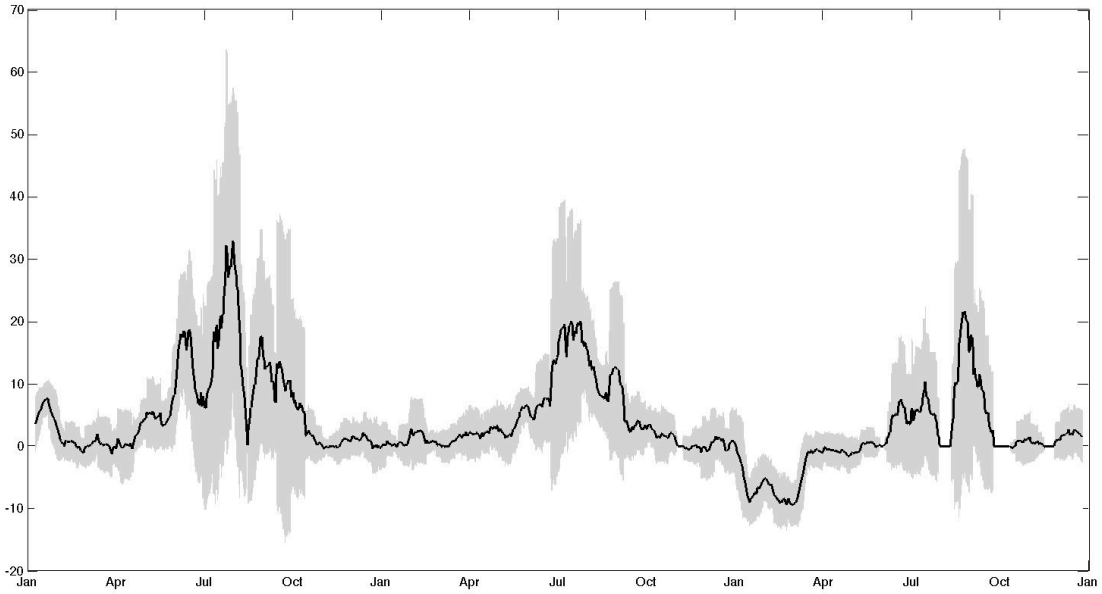

Figure 26: Fifteen-day running, daily average, methane flux in mg/m^2/day. Calculated using the modified Bowen ratio method at the WLEF site from 1997 through 1999, black, ±1 standard error, grey shading. Gaps were filled with the six-day running hourly average before daily averaging was performed.

A seasonal cycle of methane flux is seen in the MBR estimates with highly variable daily and hourly rates resulting in net emission during the summertime and slight consumption during the winter. Sharp summertime reductions to zero seen in 1997 and 1999 are spurious products of the gap filling scheme. The period of significant consumption during the winter of 1999 was omitted by [*Werner et al.*, 2003] as erroneous, along with 71%, 66% and 54% of the measurements made in 1997, 1998 and 1999 respectively. These values had anomalous CO_2 fluxes (>40 μmol/m^2/s), abnormally high ratios of the gradient of CH_4 and CO_2 (≥0.15), or friction velocities too low for the flux to be determined (<0.23 m/s). These exclusions are not here made, gaps result only

from instrument failure, as a result the fluxes and particularly their standard error differ from the previously reported values.

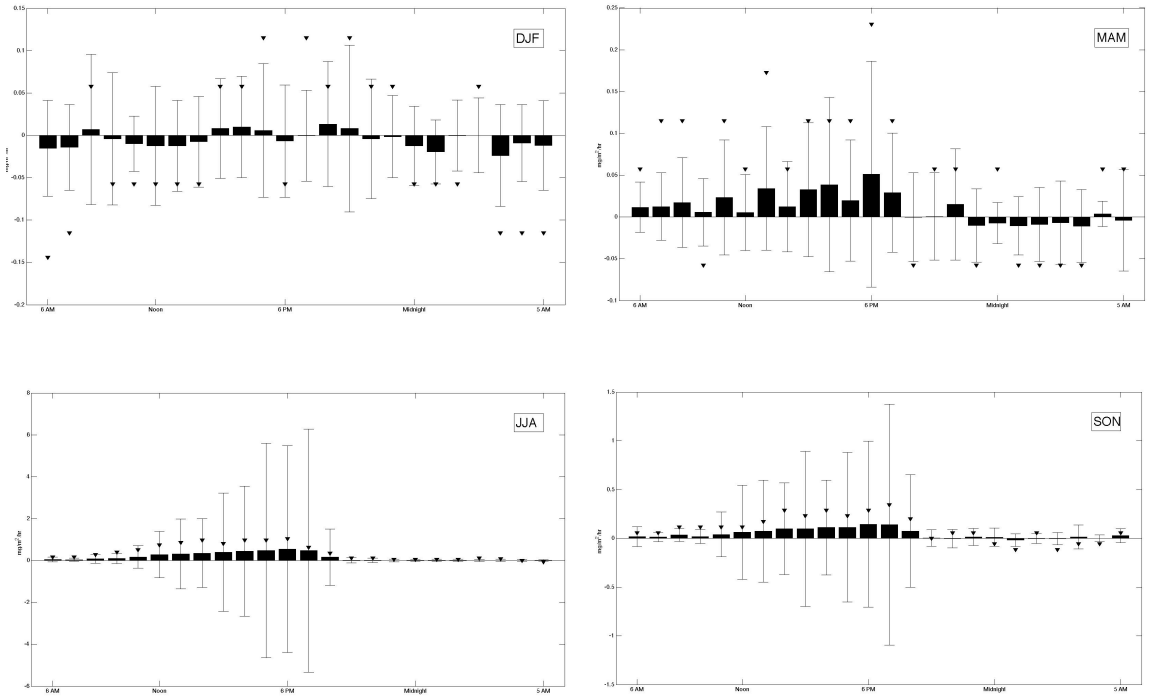

Figure 27: Composite diurnal cycles for each season of the MBR estimates. Bars indicate the mean methane flux, stems span ±1 standard error, triangles indicate the median all in mg/m^2. Gaps were ignored in the averaging. Note variation in the range of the y-axis in each panel.

Three-year seasonal composite diurnal cycles of the MBR estimates show near zero fluxes in the spring, MAM, and winter, DJF. During these periods median fluxes commonly differed from mean values, indicating considerable influence of outliers on the mean values. No pattern is seen the spring medians, but the wintertime medians are consistently higher the the mean, indicating that the outliers are most frequently periods of methane uptake. In spring, a weak trend toward daytime emission and nighttime uptake may be seen, this pattern is consistent with temperature mediated flux.

Net positive fluxes are observed in the summer, JJA, and fall, SON. Large standard errors indicate frequent anomalies, and median values concordant with the means indicates these may be of either sign. Consistently large mean and medial summer daytime fluxes suggest a temperature dependent diurnal cycle, with anomalies resulting from advection of CH_4 enriched air at the upper measurement level. This interpretation is also applicable to the fall, where a moderate trend toward daytime emission and nighttime consumption further suggests regulation by temperature.

Appropriate comparison between modeled and observed fluxes must include some modeling of gas transport. Sub-surface transport mechanisms may be of considerable importance to estimating atmospheric flux [*Walter and Heimann*, 2000], [*Grant and Roulet*, 2002], but these are not here treated. Atmospheric transport of methane through the canopy air space is implemented in SiB. Fluxes of methane are calculated as described in the previous section, using a $Q_{10P} = 5$. Fluxes are added to the canopy air space concentration of methane, expressed as a partial pressure. Negative fluxes may result in negative canopy air space concentrations, these are permitted following the rational by which methanotrophy was unlimited. The gradient of partial pressure between the reference level and the canopy air space is then calculated using a constant reference level partial pressure of 0.181372 hPa, equivalent to the average global atmospheric methane concentration of 1.79 ppm [*Dlugokencky et al.*, 2009]. The exchange of methane is then given as

$$CH_4 exchange = tc \cdot \left(\delta CH_4\right), \tag{29}$$

where *tc*, is the transfer coefficient of the turbulent flux of air out of the canopy air space into the reference level. This coefficient is a parameterized function of the temperatures and pressures of the reference level and the canopy air space, the reference level wind speed and the roughness coefficients for the biome.

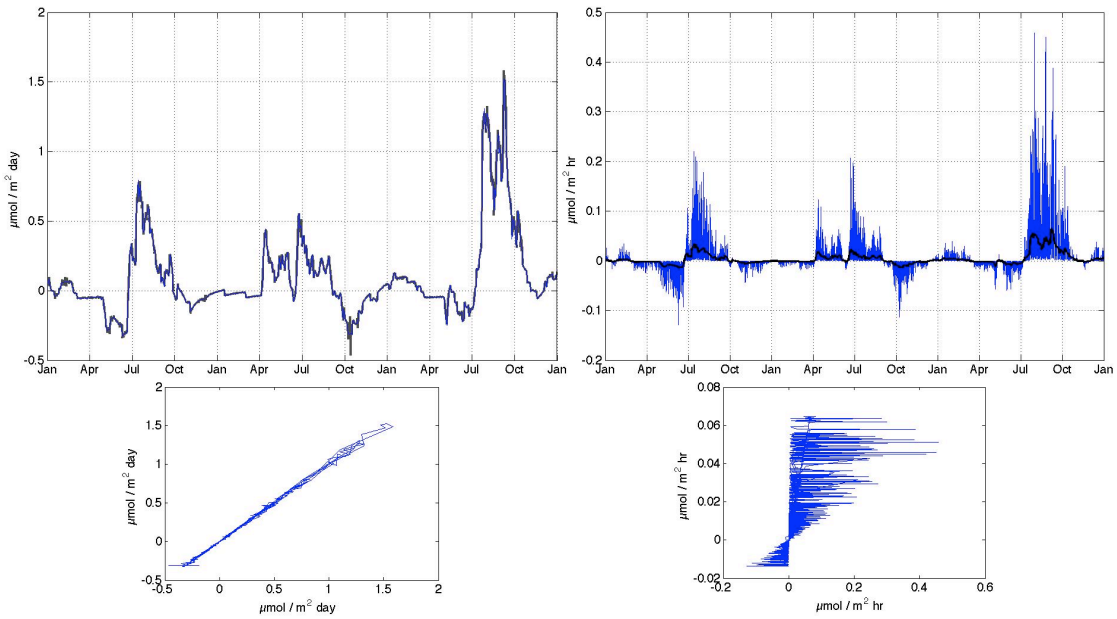

Figure 28: Modeled flux of methane to the canopy air space in black, and modeled exchange of methane with the reference layer in blue. Daily fluxes are shown in the upper left, hourly fluxes in the upper right. Below, flux to the canopy air space is plotted as a function of flux to the reference layer.

The exchange of methane between the canopy air space and the reference layer fluctuates quickly from hour to hour, but total daily fluxes and exchanges are almost identical. This is the expected behavior, the model should not allow the canopy air to remain stagnant throughout an entire day.

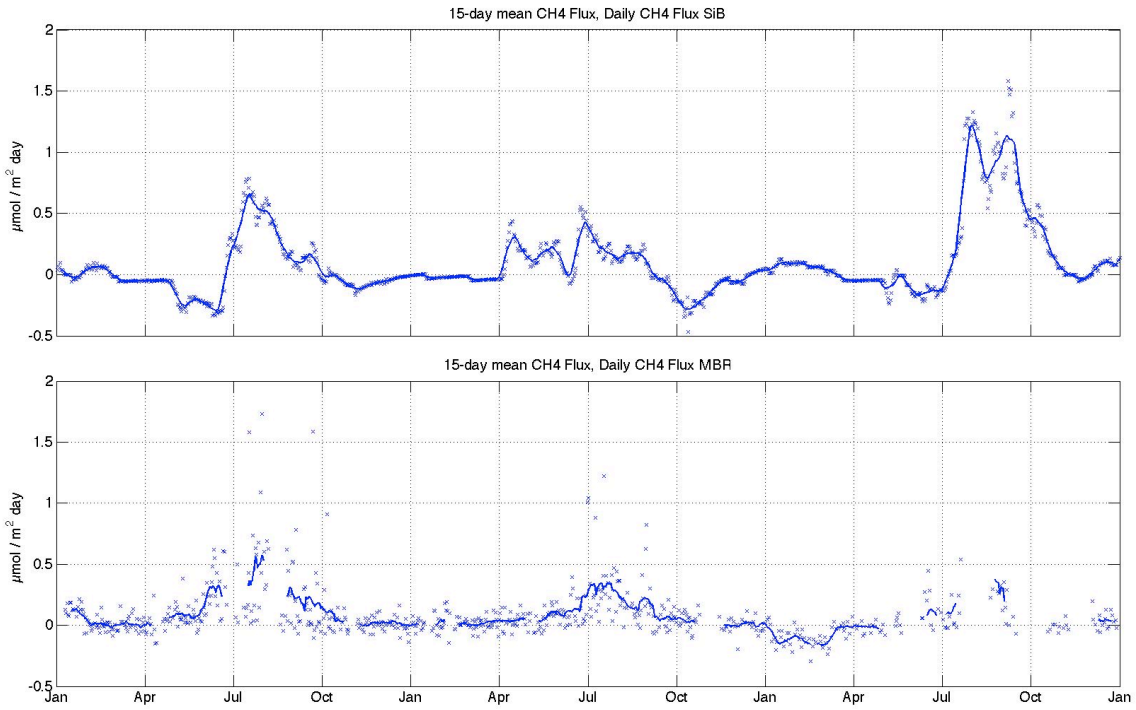

Figure 29: Modeled exchange of methane with the reference layer (above) and MBR estimated flux of methane (below) in μmol/m^2/day. Lines show the fifteen running average and crosses mark the net daily flux. The mean methane flux is not reported when more than seven days are missing from the averaging period, days are considered missing if more then 12 hourly measurements are missing, otherwise gaps are ignored in the summations and averaging.

The MBR estimates exhibit greater variability than the model year round, and dramatically more variation in the summer. Spring and fall fluxes, hypothesized and modeled as negative are positive in the fifteen-day mean MBR estimates, although negative daily values are frequently observed during those times. Mean negative fluxes are rarely seen the MBR estimates, contrary to expectation, and those that are seen are most common during the winter.

Discrepancy between modeled and MBR estimates may result from either the differences between the modeled and observed turbulent flux or the differences between

the modeled and observed methane concentrations. Motivated by interest is the methane model and the wetland area model underlying it, estimates of methane flux are recalculated by replacing $Flux_{CO2\text{-}30m}$ in equation (29) with the CO_2 flux calculated in SiB. MBR estimates driven with SiB's turbulent flux compared to the original MBR estimates indicates physical discrepancies, and compared to the model estimates indicated biological discrepancies.

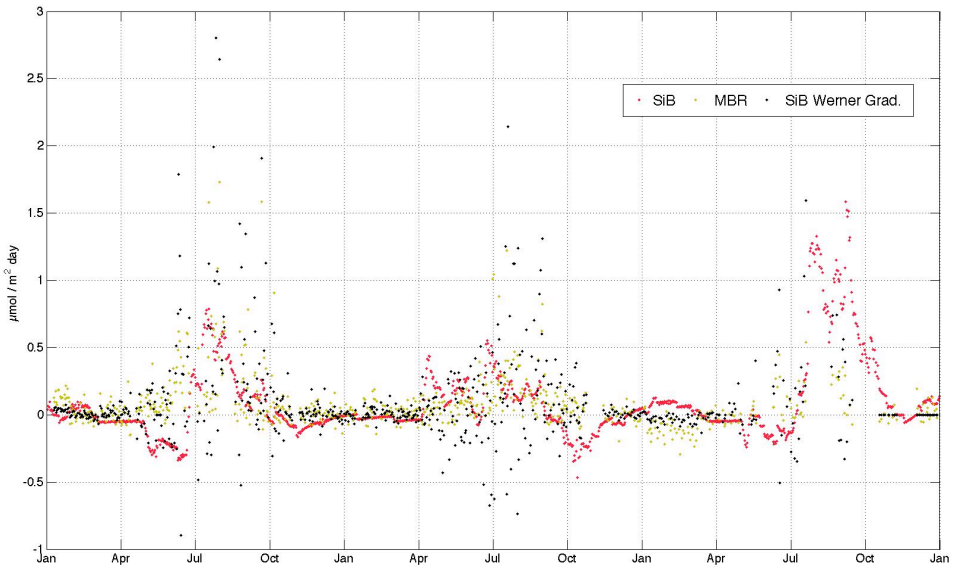

Figure 30: Methane exchange in μmol/m^2/day at the WLEF site from 1997 through 1999. Modeled net daily exchange of methane in red, the original MBR estimates of methane flux in yellow and MBR estimates calculated using SiB CO_2 flux and measured concentrations in black.

Employing SiB's turbulent fluxes increases the variability of the estimates, but better agreement with model predictions is found particularly in the spring of 1997 where the number and magnitude of negative fluxes were increased in line with expectation and model predictions. Similar, though less conspicuous patterns are seen in fall of 1997 and perhaps also in spring of 1999 although in that case data was sparse. Modeled positive

springtime fluxes in 1998 are also more consistent with MBR estimates using SiB's turbulent flux.

Model overestimates of methane uptake during the spring and fall stem from consistent predictions of negative flux of the correct magnitude. This suggests that the parameterization of the model is accurate, at least for the WLEF site over this time period, but the structure of the model is flawed in allowing methanotrophy to proceed independently from methane concentration.

January and February of 1999 are anomalous both the in model and the original MBR estimates, but the deviations are of opposite sign. The anomaly is reduced with the use of SiB fluxes, but values are still negative. Model predictions of methane emission during this period are associated with large wetland fractions a result of unusually high surface temperatures and an early snowmelt. Measurements in this period were discarded by [*Werner et al.*, 2003], but the motivation for doing so was not specified.

Negative daily values in the summertime are seen frequently in the MBR estimates using SiB flux, occasionally in the original MBS fluxes and almost never in the model. This behavior in the MBR estimates likely results from the advection of methane rich air producing high methane concentrations at the upper measurement level. Modeling of this phenomena would require variability in the reference level methane concentration and therefore an atmosphere-coupled regional or global model run.

REFERENCES

Ambroise, B., K. Beven, and J. Freer (1996), Toward a generalization of the TOPMODEL concepts: Topographic indices of hydrological similarity, *Water Resour Res*, *32*(7), 2135-2145.

Anderson, B., K. Bartlett, S. Frolking, K. Hayhoe, J. Jenkins, and W. Salas (2010), *Methane and Nitrous Oxide Emissions From Natural Sources*, United States Environmental Protection Agency, Washington, DC.

Arnold, N. A. N. (2011), A new approach for dealing with depressions in digital elevation models when calculating flow accumulation values (vol 34, pg 781, 2010), *Progress in Physical Geography*, *35*(2), 273-273.

Aselmann, I., and P. J. Crutzen (1989), Global Distribution of Natural Fresh-Water Wetlands and Rice Paddies, Their Net Primary Productivity, Seasonality and Possible Methane Emissions, *J Atmos Chem*, *8*(4), 307-358.

Aydin, M., K. R. Verhulst, E. S. Saltzman, M. O. Battle, S. A. Montzka, D. R. Blake, Q. Tang, and M. J. Prather (2011), Recent decreases in fossil-fuel emissions of ethane and methane derived from firn air, *Nature*, *476*(7359), 198-201.

Baker, I. T., A. S. Denning, and R. Stöckli (2010), North American gross primary productivity: regional characterization and interannual variability, *Tellus B*, *62*(5), 533-549.

Baker, I. T., L. Prihodko, A. S. Denning, M. Goulden, S. Miller, and H. R. da Rocha (2008), Seasonal drought stress in the Amazon: Reconciling models and observations, *J. Geophys. Res.*, *113*(G1), G00B01.

Baker, I. T., A. S. Denning, N. Hanan, L. Prihodko, M. Uliasz, P. L. Vidale, K. Davis, and P. Bakwin (2003), Simulated and observed fluxes of sensible and latent heat and CO2 at the WLEF-TV tower using SiB2.5, *Global Change Biol*, *9*(9), 1262-1277.

Beven, K., and M. Kirkby (1979), A physically based, variable contributing area model of basin hydrology, *Bulletin of the International Association of Scientific Hydrology*, *24*(1), 43-69.

Beven, K., R. Lamb, P. Quinn, R. Romanowicz, and J. Freer (1995), *TOPMODEL*, Water Resources Publications, Highlands Ranch, CO.

Bloom, A. A., P. I. Palmer, A. Fraser, D. S. Reay, and C. Frankenberg (2010), Large-Scale Controls of Methanogenesis Inferred from Methane and Gravity Spaceborne Data, *Science*, *327*(5963), 322-325.

Bohn, T. J., D. P. Lettenmaier, K. Sathulur, L. C. Bowling, E. Podest, K. C. McDonald, and T. Friborg (2007), Methane emissions from western Siberian wetlands: heterogeneity and sensitivity to climate change, *Environ Res Lett*, *2*(4), -.
Bousquet, P., D. A. Hauglustaine, P. Peylin, C. Carouge, and P. Ciais (2005), Two decades of OH variability as inferred by an inversion of atmospheric transport and chemistry of methyl chloroform, *Atmos Chem Phys*, *5*, 2635-2656.
Bousquet, P., et al. (2006), Contribution of anthropogenic and natural sources to atmospheric methane variability, *Nature*, *443*(7110), 439-443.
Bridgham, S. D., J. P. Megonigal, J. K. Keller, N. B. Bliss, and C. Trettin (2006), The carbon balance of North American wetlands, *Wetlands*, *26*(4), 889-916.
Cao, M. K., S. Marshall, and K. Gregson (1996), Global carbon exchange and methane emissions from natural wetlands: Application of a process-based model, *J. Geophys. Res.*, *101*(D9), 14399-14414.
Cao, M. K., K. Gregson, and S. Marshall (1998), Global methane emission from wetlands and its sensitivity to climate change, *Atmos Environ*, *32*(19), 3293-3299.
Chen, J., and P. Kumar (2001), Topographic influence on the seasonal and interannual variation of water and energy balance of basins in North America, *J Climate*, *14*(9), 1989-2014.
Cicerone, R. J., and R. S. Oremland (1988), Biogeochemical aspects of atmospheric methane, *Global Biogeochem. Cycles*, *2*(4), 299-327.
Clapp, R. B., and G. M. Hornberger (1978), Empirical Equations for Some Soil Hydraulic-Properties, *Water Resour Res*, *14*(4), 601-604.
Collatz, G. J., J. T. Ball, C. Grivet, and J. A. Berry (1991), Physiological and environmental regulation of stomatal conductance, photosynthesis and transpiration: a model that includes a laminar boundary layer, *Agr Forest Meteorol*, *54*(2-4), 107-136.
Cui, J. B., C. S. Li, G. Sun, and C. Trettin (2005), Linkage of MIKE SHE to Wetland-DNDC for carbon budgeting and anaerobic biogeochemistry simulation, *Biogeochemistry*, *72*(2), 147-167.
Curie, F., S. Gaillard, A. Ducharne, and H. Bendjoudi (2007), Geomorphological methods to characterise wetlands at the scale of the Seine watershed, *Sci Total Environ*, *375*(1-3), 59-68.
Davidson, E. A., I. A. Janssens, and Y. Luo (2006), On the variability of respiration in terrestrial ecosystems: moving beyond Q10, *Global Change Biol*, *12*(2), 154-164.
Denning, A. S., G. J. Collatz, C. G. Zhang, D. A. Randall, J. A. Berry, P. J. Sellers, G. D. Colello, and D. A. Dazlich (1996), Simulations of terrestrial carbon metabolism and atmospheric CO2 in a general circulation model .1. Surface carbon fluxes, *Tellus B*, *48* (4), 521-542.
Dlugokencky, E. J., K. A. Masarie, P. M. Lang, and P. P. Tans (1998), Continuing decline in the growth rate of the atmospheric methane burden, *Nature*, *393*(6684), 447-450.
Dlugokencky, E. J., S. Houweling, L. Bruhwiler, K. A. Masarie, P. M. Lang, J. B. Miller, and P. P. Tans (2003), Atmospheric methane levels off: Temporary pause or a new steady-state?, *Geophys Res Lett*, *30*(19), -.

Dlugokencky, E. J., et al. (2009), Observational constraints on recent increases in the atmospheric CH4 burden, *Geophys Res Lett*, *36*, -.
Duan, J. F., and N. L. Miller (1997), A generalized power function for the subsurface transmissivity profile in TOPMODEL, *Water Resour Res*, *33*(11), 2559-2562.
Ducharne, A. (2009), Reducing scale dependence in TOPMODEL using a dimensionless topographic index, *Hydrol Earth Syst Sc*, *13*(12), 2399-2412.
Ducharne, A., R. D. Koster, M. J. Suarez, and P. Kumar (1999), A catchment-based land surface model for GCMs and the framework for its evaluation, *Phys Chem Earth Pt B*, *24* (7), 769-773.
Ducharne, A., R. D. Koster, M. J. Suarez, M. Stieglitz, and P. Kumar (2000), A catchment-based approach to modeling land surface processes in a general circulation model 2. Parameter estimation and model demonstration, *J Geophys Res-Atmos*, *105* (D20), 24823-24838.
Eliseev, A., I. Mokhov, M. Arzhanov, P. Demchenko, and S. Denisov (2008), Interaction of the methane cycle and processes in wetland ecosystems in a climate model of intermediate complexity, *Izvestiya Atmospheric and Oceanic Physics*, *44*(2), 139-152.
Erskine, R. H., T. R. Green, J. A. Ramirez, and L. H. MacDonald (2006), Comparison of grid-based algorithms for computing upslope contributing area, *Water Resour. Res.*, *42* (9), W09416.
Farquhar, G. D., S. Caemmerer, and J. A. Berry (1980), A biochemical model of photosynthetic CO₂ assimilation in leaves of C₃ species, *Planta*, *149*(1), 78-90.
Franchini, M., J. Wendling, C. Obled, and E. Todini (1996), Physical interpretation and sensitivity analysis of the TOPMODEL, *J Hydrol*, *175*(1-4), 293-338.
Frey, K. E., and L. C. Smith (2007), How well do we know northern land cover? Comparison of four global vegetation and wetland products with a new ground-truth database for West Siberia, *Global Biogeochem Cy*, *21*(1), -.
Friborg, T., T. R. Christensen, B. U. Hansen, C. Nordstroem, and H. Soegaard (2000), Trace gas exchange in a high-arctic valley 2. Landscape CH4 fluxes measured and modeled using eddy correlation data, *Global Biogeochem Cy*, *14*(3), 715-723.
Gedney, N., and P. M. Cox (2003), The sensitivity of global climate model simulations to the representation of soil moisture heterogeneity, *J Hydrometeorol*, *4*(6), 1265-1275.
Gedney, N., P. M. Cox, and C. Huntingford (2004), Climate feedback from wetland methane emissions, *Geophys Res Lett*, *31*(20), -.
Gesch, D. (2007), The National Elevation Dataset, in *Digital Elevation Model Technologies and Applications: The DEM Users Manual, 2nd Edition*, edited by D. Maune, pp. p. 99-118, American Society for Photogrammetry and Remote Sensing, Bethesda, MD.
Gesch, D., M. Oimoen, S. Greenlee, C. Nelson, M. Steuck, and D. Tyler (2002), The National Elevation Dataset, *Photogramm Eng Rem S*, *68*(1), 5-11.
Grant, R. F., and N. T. Roulet (2002), Methane efflux from boreal wetlands: Theory and testing of the ecosystem model Ecosys with chamber and tower flux measurements, *Global Biogeochem Cy*, *16*(4), -.

Güntner, A., J. Seibert, and S. Uhlenbrook (2004), Modeling spatial patterns of saturated areas: An evaluation of different terrain indices, *Water Resour. Res.*, *40*(5), W05114.
Güntner, A., S. Uhlenbrook, J. Seibert, and C. Leibundgut (1999), Multi-criterial validation of TOPMODEL in a mountainous catchment, *Hydrol Process*, *13*(11), 1603-1620.
Hargreaves, K. J., D. Fowler, C. E. R. Pitcairn, and M. Aurela (2001), Annual methane emission from Finnish mires estimated from eddy covariance campaign measurements, *Theoretical and Applied Climatology*, *70*(1), 203-213.
Homer, C., C. Huang, L. Yang, W. B., and C. M. (2001), NLCD 2001 Land Cover Version 2.0, edited by U. S. G. Survey, Sioux Falls, SD.
IPCC (Ed.) (2007), *Climate Change 2007: The Physical Science Basis. Contribution of Working Group I to the Fourth Assessment Report of the Intergovernmental Panel on Climate Change*, 996 pp., Cambridge University Press, Cambridge, United Kingdom and New York, NY, USA.
Jenson, S. K., and J. O. Domingue (1988), Extracting Topographic Structure from Digital Elevation Data for Geographic Information-System Analysis, *Photogramm Eng Rem S*, *54*(11), 1593-1600.
Kai, F. M., S. C. Tyler, J. T. Randerson, and D. R. Blake (2011), Reduced methane growth rate explained by decreased Northern Hemisphere microbial sources, *Nature*, *476* (7359), 194-197.
Koster, R. D., M. J. Suarez, A. Ducharne, M. Stieglitz, and P. Kumar (2000), A catchment-based approach to modeling land surface processes in a general circulation model 1. Model structure, *J Geophys Res-Atmos*, *105*(D20), 24809-24822.
Lehner, B., and P. Döll (2004), Development and validation of a global database of lakes, reservoirs and wetlands, *J Hydrol*, *296*(1-4), 1-22.
Leibowitz, S. G., and T. L. Nadeau (2003), Isolated wetlands: State-of-the-science and future directions, *Wetlands*, *23*(3), 663-684.
Lelieveld, J., P. J. Crutzen, and F. J. Dentener (1998), Changing concentration, lifetime and climate forcing of atmospheric methane, *Tellus B*, *50*(2), 128-150.
Li, C., J. Qiu, S. Frolking, X. Xiao, W. Salas, B. Moore, III, S. Boles, Y. Huang, and R. Sass (2002), Reduced methane emissions from large-scale changes in water management of China's rice paddies during 1980-2000, *Geophys. Res. Lett.*, *29*(20), 1972.
Lindsay, J. B., and I. F. Creed (2005), Removal of artifact depressions from digital elevation models: towards a minimum impact approach, *Hydrol Process*, *19*(16), 3113-3126.
Liu, J. (2004), Investigation of Ecosystem Drought Stress and its Impacts on Carbon Exchange in Tropical Forests, 105 pp, Colorado State University, Fort Collins, CO.
Long, K. D., L. B. Flanagan, and T. Cai (2010), Diurnal and seasonal variation in methane emissions in a northern Canadian peatland measured by eddy covariance, *Global Change Biol*, *16*(9), 2420-2435.
MacKay, D. S., D. E. Ahl, B. E. Ewers, S. T. Gower, S. N. Burrows, S. Samanta, and K. J. Davis (2002), Effects of aggregated classifications of forest composition on estimates of

evapotranspiration in a northern Wisconsin forest, *Global Change Biol*, *8*(12), 1253-1265.
Manning, M. R., D. C. Lowe, R. C. Moss, G. E. Bodeker, and W. Allan (2005), Short-term variations in the oxidizing power of the atmosphere, *Nature*, *436*(7053), 1001-1004.
Matthews, E., and I. Fung (1987), Methane emission from natural wetlands: Global distribution, area, and environmental characteristics of sources, *Global Biogeochem. Cycles*, *1*(1), 61-86.
Merot, P., B. Ezzahar, C. Walter, and P. Aurousseau (1995), Mapping waterlogging of soils using digital terrain models, *Hydrol Process*, *9*(1), 27-34.
Merot, P., H. Squividant, P. Aurousseau, M. Hefting, T. Burt, V. Maitre, M. Kruk, A. Butturini, C. Thenail, and V. Viaud (2003), Testing a climato-topographic index for predicting wetlands distribution along an European climate gradient, *Ecol Model*, *163* (1-2), 51-71.
Mikaloff Fletcher, S. E., P. P. Tans, L. M. Bruhwiler, J. B. Miller, and M. Heimann (2004), CH4 sources estimated from atmospheric observations of CH4 and its 13C/12C isotopic ratios: 1. Inverse modeling of source processes, *Global Biogeochem. Cycles*, *18* (4), GB4004.
Mitsch, W. J., and J. G. Gosselink (2007), *Wetlands, 4th edition*, John Wiley & Sons, Inc.
Montzka, S. A., M. Krol, E. Dlugokencky, B. Hall, P. J√∂ckel, and J. Lelieveld (2011), Small Interannual Variability of Global Atmospheric Hydroxyl, *Science*, *331*(6013), 67-69.
Murphy, P. N. C., J. Ogilvie, and P. Arp (2009), Topographic modelling of soil moisture conditions: a comparison and verification of two models, *Eur J Soil Sci*, *60*(1), 94-109.
Murphy, P. N. C., J. Ogilvie, K. Connor, and P. A. Arpl (2007), Mapping wetlands: A comparison of two different approaches for New Brunswick, Canada, *Wetlands*, *27*(4), 846-854.
Niu, G. Y., Z. L. Yang, R. E. Dickinson, and L. E. Gulden (2005), A simple TOPMODEL-based runoff parameterization (SIMTOP) for use in global climate models, *J Geophys Res-Atmos*, *110*(D21), -.
Owe, M., R. de Jeu, and T. Holmes (2008), Multisensor historical climatology of satellite-derived global land surface moisture, *J. Geophys. Res.*, *113*(F1), F01002.
Papa, F., C. Prigent, F. Aires, C. Jimenez, W. B. Rossow, and E. Matthews (2010), Interannual variability of surface water extent at the global scale, 1993-2004, *J Geophys Res-Atmos*, *115*, -.
Potter, C. (1997), An ecosystem simulation model for methane production and emission from wetlands, *Global Biogeochem Cy*, *11*(4), 495-506.
Potter, C., S. Klooster, S. Hiatt, M. Fladeland, V. Genovese, and P. Gross (2006), Methane Emissions from Natural Wetlands in the United States: Satellite-Derived Estimation Based on Ecosystem Carbon Cycling, *Earth Interact*, *10*(22), 1-12.
Prigent, C., F. Aires, W. B. Rossow, and E. Matthews (2001a), Joint characterization of vegetation by satellite observations from visible to microwave wavelengths: A sensitivity analysis, *J. Geophys. Res.*, *106*(D18), 20665-20685.

Prigent, C., E. Matthews, F. Aires, and W. B. Rossow (2001b), Remote sensing of global wetland dynamics with multiple satellite data sets, *Geophys Res Lett*, *28*(24), 4631-4634.
Prigent, C., F. Papa, F. Aires, W. B. Rossow, and E. Matthews (2007), Global inundation dynamics inferred from multiple satellite observations, 1993-2000, *J Geophys Res-Atmos*, *112*(D12), -.
Prinn, R. G., et al. (2005), Evidence for variability of atmospheric hydroxyl radicals over the past quarter century, *Geophys. Res. Lett.*, *32*(7), L07809.
Quinn, P., K. Beven, and R. Lamb (1995), The Ln(a/Tan-Beta) Index - How to Calculate It and How to Use It within the Topmodel Framework, *Hydrol Process*, *9*(2), 161-182.
Quinn, P., K. Beven, P. Chevallier, and O. Planchon (1991), The prediction of hillslope flow paths for distributed hydrological modelling using digital terrain models, *Hydrol Process*, *5*(1), 59-79.
Rasmussen, R. A., and M. A. K. Khalil (1984), Atmospheric Methane in the Recent and Ancient Atmospheres: Concentrations, Trends, and Interhemispheric Gradient, *J. Geophys. Res.*, *89*(D7), 11599-11605.
Reay, D., P. Smith, and A. van Amstel (2010), Methane and Climate Change, edited, Earthscan, London.
Reddy, K. R., and R. D. DeLaune (2008), *Biogeochemistry of Wetlands: Science and Applications*, CRC Press.
Rigby, M., et al. (2008), Renewed growth of atmospheric methane, *Geophys Res Lett*, *35* (22), -.
Ringeval, B., N. de Noblet-Ducoudré, P. Ciais, P. Bousquet, C. Prigent, F. Papa, and W. B. Rossow (2010), An attempt to quantify the impact of changes in wetland extent on methane emissions on the seasonal and interannual time scales, *Global Biogeochem. Cycles*, *24*(2), GB2003.
Rinne, J., T. Riutta, M. Pihlatie, M. Aurela, S. Haapanala, J.-P. Tuovinen, E.-S. Tuittila, and T. Vesala (2007), Annual cycle of methane emission from a boreal fen measured by the eddy covariance technique, *Tellus B*, *59*(3), 449-457.
Rodhe, A., and J. Seibert (1999), Wetland occurrence in relation to topography: a test of topographic indices as moisture indicators, *Agr Forest Meteorol*, *98-9*, 325-340.
Sachs, T., M. Giebels, J. Boike, and L. Kutzbach (2010), Environmental controls on CH4 emission from polygonal tundra on the microsite scale in the Lena river delta, Siberia, *Global Change Biol*, *16*(11), 3096-3110.
Schaefer, K., T. Zhang, A. G. Slater, L. Lu, A. Etringer, and I. Baker (2009), Improving simulated soil temperatures and soil freeze/thaw at high-latitude regions in the Simple Biosphere/Carnegie-Ames-Stanford Approach model, *J. Geophys. Res.*, *114*(F2), F02021.
Segers, R. (1998), Methane production and methane consumption: a review of processes underlying wetland methane fluxes, *Biogeochemistry*, *41*(1), 23-51.
Sellers, P. J., Y. Mintz, Y. C. Sud, and A. Dalcher (1986), A Simple Biosphere Model (Sib) for Use within General-Circulation Models, *J Atmos Sci*, *43*(6), 505-531.
Sellers, P. J., D. A. Randall, G. J. Collatz, J. A. Berry, C. B. Field, D. A. Dazlich, C. Zhang, G. D. Collelo, and L. Bounoua (1996), A revised land surface parameterization (SiB2) for atmospheric GCMs .1. Model formulation, *J Climate*, *9*(4), 676-705.

Simpson, I. J., F. S. Rowland, S. Meinardi, and D. R. Blake (2006), Influence of biomass burning during recent fluctuations in the slow growth of global tropospheric methane, *Geophys Res Lett*, *33*(22), -.
Sivapalan, M., K. Beven, and E. F. Wood (1987), On Hydrologic Similarity .2. A Scaled Model of Storm Runoff Production, *Water Resour Res*, *23*(12), 2266-2278.
Stieglitz, M., D. Rind, J. Famiglietti, and C. Rosenzweig (1997), An efficient approach to modeling the topographic control of surface hydrology for regional and global climate modeling, *J Climate*, *10*(1), 118-137.
Stockli, R., P. L. Vidale, A. Boone, and C. Schar (2007), Impact of scale and aggregation on the terrestrial water exchange: Integrating land surface models and Rhone catchment observations, *J Hydrometeorol*, *8*(5), 1002-1015.
Tiner, R. W. (1999), *Wetland Indicators: A Guide to Wetland Identification, Delineation, Classification, and Mapping*, Lewis Publishers, New York.
Verdin, K. L., and J. P. Verdin (1999), A topological system for delineation and codification of the Earth's river basins, *J Hydrol*, *218*(1-2), 1-12.
Vidale, P. L., and R. Stöckli (2005), Prognostic canopy air space solutions for land surface exchanges, *Theoretical and Applied Climatology*, *80*(2), 245-257.
von Fischer, J. C., and L. O. Hedin (2007), Controls on soil methane fluxes: Tests of biophysical mechanisms using stable isotope tracers, *Global Biogeochem Cy*, *21*(2), -.
Walko, R. L., et al. (2000), Coupled atmosphere-biophysics-hydrology models for environmental modeling, *J Appl Meteorol*, *39*(6), 931-944.
Walter, B. P., and M. Heimann (2000), A process-based, climate-sensitive model to derive methane emissions from natural wetlands: Application to five wetland sites, sensitivity to model parameters, and climate, *Global Biogeochem Cy*, *14*(3), 745-765.
Walter, B. P., M. Heimann, and E. Matthews (2001), Modeling modern methane emissions from natural wetlands 2. Interannual variations 1982-1993, *J Geophys Res-Atmos*, *106*(D24), 34207-34219.
Walter, B. P., M. Heimann, R. D. Shannon, and J. R. White (1996), A process-based model to derive methane emissions from natural wetlands, *Geophys Res Lett*, *23*(25), 3731-3734.
Werner, C., K. Davis, P. Bakwin, C. X. Yi, D. Hurst, and L. Lock (2003), Regional-scale measurements of CH4 exchange from a tall tower over a mixed temperate/boreal lowland and wetland forest, *Global Change Biol*, *9*(9), 1251-1261.
Western, A. W., R. B. Grayson, G. Bloschl, G. R. Willgoose, and T. A. McMahon (1999), Observed spatial organization of soil moisture and its relation to terrain indices, *Water Resour Res*, *35*(3), 797-810.
Whalen, S. C. (2005), Biogeochemistry of methane exchange between natural wetlands and the atmosphere, *Environ Eng Sci*, *22*(1), 73-94.
Whiting, G. J., and J. P. Chanton (1993), Primary Production Control of Methane Emission from Wetlands, *Nature*, *364*(6440), 794-795.
Wille, C., L. Kutzbach, T. Sachs, D. Wagner, and E.-M. Pfeiffer (2008), Methane emission from Siberian arctic polygonal tundra: eddy covariance measurements and modeling, *Global Change Biol*, *14*(6), 1395-1408.

Wolock, D. M., and C. V. Price (1994), Effects of Digital Elevation Model Map Scale and Data Resolution on a Topography-Based Watershed Model, *Water Resour Res*, *30*(11), 3041-3052.
Wolock, D. M., and G. J. McCabe (2000), Differences in topographic characteristics computed from 100- and 1000-m resolution digital elevation model data, *Hydrol Process*, *14*(6), 987-1002.
Wuebbles, D. J., and K. Hayhoe (2002), Atmospheric methane and global change, *Earth-Sci Rev*, *57*(3-4), 177-210.
Zhang, Y., C. S. Li, C. C. Trettin, H. Li, and G. Sun (2002), An integrated model of soil, hydrology, and vegetation for carbon dynamics in wetland ecosystems, *Global Biogeochem Cy*, *16*(4), -.
Zhuang, Q., J. M. Melillo, D. W. Kicklighter, R. G. Prinn, A. D. McGuire, P. A. Steudler, B. S. Felzer, and S. Hu (2004), Methane fluxes between terrestrial ecosystems and the atmosphere at northern high latitudes during the past century: A retrospective analysis with a process-based biogeochemistry model, *Global Biogeochem Cy*, *18*(3), -.